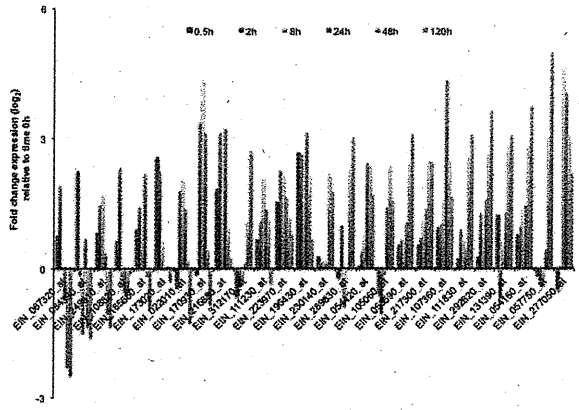

Figure 2. Modulation of the transcript level of the *E. invadens* BspA- like genes during encystation. Values are expressed as $\log_2$ fold change of expression relative to time 0 h.

doi: 10.1371/journal.pone.0074840.g002

in high and low iron concentrations [35]. In *E. histolytica*, iron and serum starvation resulted in the trafficking of a cytoplasmic EhRab11A protein to the cell periphery and the development of detergent resistance, similar to the cyst stage [36]. It would be interesting to show the localization of *E. invadens* BspA in encysting cells to determine its possible function during encystation.

B: Cytoskeletal proteins

The Rho/Rac family of small GTP binding proteins is known to be involved in cytoskeleton regulation [37]. Two *E. invadens*-specific (i.e., no homolog in *E. histolytica*) *Rac* genes (EIN_166990 and EIN_017340) were modulated at early time points (Table S1), while one *RacJ* (EIN_243630) and one *RacD* (EIN_137540) genes, which also have *E. histolytica* counterparts, were up-regulated at late time points together with several Rho/Rac effectors [GTPase activating proteins (GAP) and guanine nucleotide exchange factors (GEF)]. In *E. histolytica*, it was previously shown that only a gene encoding for RacH, whose physiological role has not yet been established, was up-regulated specifically in cysts [12]. A homolog of *RacH* gene (EIN_105260) showed slight change (2 fold) in gene expression at 0.5 h of encystation (Table S1). These data are consistent with the notion that regulation of cytoskeletal rearrangement is essential at the early phase of encystation when trophozoites rearrange its surface for aggregation. It was also shown that cytochalasin D, a potent inhibitor of actin polymerization, inhibits encystation [38].

Phosphoinositides such as phosphatidylinositol 4,5-bisphosphate [PtdIns(4,5) P2] are important secondary messengers in cell surface receptor-mediated signal transduction and participate in actin cytoskeleton rearrangement [37]. The enzyme phosphatidyl 3-kinase (PI3K), which phosphorylates PtdIns, was previously shown to participate in the encystation process [13,14,39]. Our transcriptome data showed the mRNA level of one *PI3K* genes (EIN_083000) increased >3 fold at 24 to 120 h of encystation (Table S6). Furthermore, genes encoding PI(4,5) P2,3-kinase (EIN_310690) and diacylglycerol kinase (EIN_196180) were also up-regulated at later time points (Tables S6 and S7). The involvement of the pathway in encystation and excystation was previously suggested [39,40]. Recently, phosphoinositides, particularly PtdIns3P and PtdIns4P, were shown to participate in cytoskeletal rearrangement during phagocytosis of *E. histolytica* [41].

C: Kinases and phosphatases

Tyrosine kinases play a pivotal role in sensing changes in the environment. It has been previously shown by analyzing transcriptome of recent clinical *E. histolytica* isolates that at least 14 transmembrane kinases (TMKs) are developmentally regulated [12]. Modulation of 8 TMKs were also observed *in vivo* [20]. Recently, analysis of *E. histolytica* TMK 39, 54, and 96 have shown to be involved in phagocytosis and growth [42,43]. Similarly, we identified 16 up-regulated *E. invadens* genes that showed significant similarity to 11 genes encoding *E. histolytica* TMKs (Table S8). Six of them were up-regulated at the early time points (*TMK 87*, Tables S4 and S5), while ten were up-regulated at the later time points (Tables S6 and S7). Forty-six *E. histolytica TMK* genes were not detected to be transcribed in trophozoites, similar to the three major cyst-specific Jacob proteins [44]. Among the *E. invadens* homologs corresponding to these 46 *E. histolytica TMK* genes, five *E. invadens TMK* gene homologs (8, 40, 38, 73, and 82) were up-regulated in later time points of encystation. However, in contrast to the previous finding, which suggested that TMK54 is involved in growth and surface expression of Gal/GalNAc lectin in trophozoites of *E. histolytica* [43], *E. invadens TMK 54* gene expression was not significantly modulated at early time point of encystation. These data suggest that TMK54 may have divergent functions in two species. *E. invadens TMK87* gene was shown to be up-regulated in *E. histolytica* in recent clinical isolates [12].

Genes encoding for serine/threonine protein phosphatases and dual specificity phosphatases were also increased during the late phase of encystation (Tables S6 and S7). In particular, 4 genes (EIN_221990, EIN_105320, EIN_020140, EIN_230540) encoding for the serine threonine phosphatases 2C (PP2C) were up-regulated during the late phase of encystation (Table S7). In yeast, PP2C phosphatases are implicated in attenuating phosphorylation during heat and osmotic shock [45]. Thus, up-regulation of PP2C might reflect anti-stress responses of *E. invadens* during encystation, which was reported to be induced by glucose starvation and hypo-osmotic shock [8]. However, the *E. invadens* PP2C homologs (Table S7) in *E. histolytica* (EHI_194220 and EHI_092510) were not shown to be cyst specific [12].

D: Metabolism

A majority of metabolic genes involved in central energy metabolism in general were repressed. However, despite its dormant nature, genes encoding several metabolic enzymes involved in nucleotide metabolism, energy, lipids, and

sphingolipids metabolism were still transcribed during the late phase of encystation (Tables S6 and S7). In our previous study we discussed detailed analysis of metabolisms of glycolysis, amino acid, cyst wall biosynthesis [46]. Briefly, among genes involved in chitin biosynthesis, the transcript level of a gene encoding for glucosamine-fructose-6-phosphate aminotransferase (GFAT, EIN_136750), which is the first and rate limiting enzyme of the chitin biosynthetic pathway, was increased at 24 h of encystation (Table S3). Chitin is the major components of the cyst wall and a homopolymer of β-1, 4-linked *N*-acetyl-glucosamine (GlcNAc) [47]. It was shown in *Giardia* that UDP-GlcNAc pyrophosphorylase (UAP) promotes the synthesis of GlcNAc and cyst wall filaments [16]. In addition, genes encoding for UDP-glucose 4-epimerase (UAE), glucosamine 6-phosphate N-acetyltransferases (GNA), phosphoglucosamine mutase (AGM), and glucosamine-6-phosphate isomerase (GNP) were also shown to be increased at mRNA and protein levels during encystation in *Giardia* [48]. However, in contrast to the findings in *Giardia*, genes for only GNA (EIN_036890) and one of UAPs (EIN_224560) were found significantly up-regulated during encystation of *E. invadens* (Table S3).

Three genes encoding for β-1,3-N-acetylglucosaminyltransferase, involved in glycosphingolipid and glycan biosynthesis, were up-regulated at either early (EIN_068160; Table S4) or late phase (EIN_112490 and EIN_200230; Table S6) of encystation. These enzymes participate in the transfer of GlcNAc from UDP-GlcNAc onto Gal β-3 (GlcNAc β-6) GalNAc-mucin and are therefore important in chitin biosynthesis.

E: Proteasome components, ubiquitin, and SUMO

It has been shown that expression of ubiquitin (*Ub*) gene is co-up-regulated with known cyst-specific genes during encystation. In addition, encystation was inhibited by proteasome inhibitors, suggesting that ubiquitin-proteasome activity is essential for encystation [9]. In agreement to the premise, transcription of major components of the Ub pathway such as the anaphase-promoting complex (EIN_034040), cell cycle division (EIN_192160), E2 Ub conjugating enzymes (EIN_101850), and E4 ubiquitination factor (EIN_107750) genes were up-regulated in the late phase of encystation (Tables S6 and S7). However, only *E. invadens Ub* gene (EIN_063840) in the *E. invadens* genome database was not significantly modulated during encystation process, which seems to contradict with the previous finding [9]. However, one should note that the *E. invadens Ub* gene previously shown to be up-regulated (AF016643 [9]) was only 52% identical to EIN_063840. The genes encoding for E1 Ub activating enzymes, 26S proteasome regulatory and core particle subunits (Table S1) were, though highly expressed, not significantly up-regulated during encystation. The gene encoding for ubiquitin carboxy-terminal hydrolase (EIN_243050) with a peptidase C19 motif was up-regulated at 8 to 120 h with a 67-fold peak expression at 24 h. A gene encoding for Ub-specific protease (EIN_107760) was also up-regulated at 24 to 48 h of encystation (Table S3). These de-ubiquitinating enzymes are likely required to process Ub-conjugated products, negatively regulate ubiquitination, and regenerate free Ub [49].

An antagonistic relationship has been established between the Ub system and sentrin/small ubiquitin-related modifier (SUMO) [50]. It has been shown that Ub and SUMO compete for a single modification site of an inhibitory protein involved in the signaling of the transcriptional activator nuclear factor–κB. SUMO-specific E2 (conjugating enzyme) Ubc9 inhibits NF-κB-dependent transcription in response to a variety of signals [50]. Our transcriptome data also showed an up-regulation of genes encoding SUMO-specific proteases (EIN_157340 and EIN_200450), SUMO ligases (EIN_168610 and EIN_081680), and Ubc9 (EIN_220240) on the late phase of encystation (Tables S6 and S7). It needs to be further determined whether Ub/SUMO antagonistic system is operated in *Entamoeba*, and the target substrates for ubiquitylation or sumoylation need to be identified [9].

F: Protein transporters

Genes encoding for major facilitator superfamily (MFS) transporter proteins were up-regulated at different time points: EIN_257160 and EIN_040590 at 0.5 to 2 h (Table S4), EIN_054130 at 8 h (Table S5), EIN_035840 at 24 h (Table S6) and EIN_059680 at 48 to 120 h (Table S7). In general, MFS proteins facilitate the transport across the cytoplasmic or internal membranes of a variety of substrates including ions, sugar phosphates, drugs, neurotransmitters, nucleosides, amino acids, and peptides [51]. Genes encoding for two MFS (EIN_035840 and EIN_059680) that were up-regulated at the late time points were predicted to be involved in multidrug efflux as predicted by TransportDB (http://membranetransport.org/), whereas the substrates of the MFS that was expressed at the early time points (EIN_257160 and EIN_040590) were not predicted. Two genes encoding for CorA (EIN_053430 and EIN_222130) metal ion transporters (MIT), which transport magnesium/cobalt ions, were also up-regulated at 2 h (Table S4). It was previously shown that supplementation of varying concentrations and mixtures of Mg^{2+}, Mn^{2+}, and Co^{2+} ions to PEHPS culture medium was essential for the production of "cyst-like" structure in *E. histolytica* trophozoites [52,53]. The presence of bivalent metal ions Mn^{2+} and Co^{2+} was also shown to be necessary for augmenting chitin synthase activity in encysting *E. invadens* [54] and recognized as co-factors in the synthesis of the cyst wall chitin [52]. Genes encoding chitin synthases (EIN_040930 and EIN_168780) were up-regulated >3 fold starting from 2 and 8 h, respectively, and remained up-regulated up to 120 h of encystation (Table S3). The simultaneous up-regulation of metal ion transporters and chitin synthases during encystation likely supports the previous report showing that *E. histolytica* generated chitin-like material during axenic cultivation upon supplementation of these metal ions [55].

Genes encoding other ion transporters including voltage ion superfamily (EIN_036050), P-type ATPase (EIN_153520 and EIN_051610), and resistance nodulation cell division (RND) transporter (EIN_016330) were also up-regulated at the early time points (Table S4). In contrast, six transporter genes encoding the ATP-binding cassette (ABC) superfamily

(EIN_015980, EIN_135600, EIN_103360, EIN_167910, EIN_146950, and EIN_059680) and four *importin* genes (EIN_219050, EIN_093910, EIN_040110, and EIN_069500) were up-regulated at the later time points (Table S7). A gene encoding for an ABC transporter (EIN_103360), previously reported to be expressed in a cyst-specific manner (EHI_178050), was also up-regulated [12]. Importin α subunit is known to bind to the nuclear localization signal of the proteins to be imported, whereas importin β subunit facilitates the docking of the importin-protein complex to the nuclear pore, respectively.

It remains still uncharacterized how the cyst wall proteins are transported in encysting trophozoites [11]. UDP-GlcNAc is the end product of the hexosamine biosynthesis pathway and the essential precursor of chitin. It was shown that accumulation of UDP-GlcNAc precedes chitin formation [46]. Two genes encoding for the UDP-GlcNAc transporter (EIN_294920 and EIN_248420) were not up-regulated with statistical significance, but gene expression slightly increased at 24 to 120 h of encystation (Table S1). These genes are known to be mainly involved in the transmembrane transport of nucleotides and sugars in the Golgi apparatus, which is the site of glycosylation, sulfation, and phosphorylation of proteoglycans and sphingolipids [56]. Up-regulation of genes encoding for UDP-GlcNAc transporters and chitinase genes (EIN_239240, EIN_053310, EIN_059870) (see below) simultaneously occurred in the late phase of encystation.

G: Vesicular trafficking: small GTPases and their effectors

E. invadens possesses 121 *Rab* genes, which were previously designated [28]. Of these 121 *Rab* genes, 14 genes (Figure 3) including 7 genes encoding RabX isotypes, which have corresponding homologs in *E. histolytica*, and 5 genes encoding *E. invadens*-specific (i.e., no homolog in *E. histolytica*) RabZ were up-regulated during encystation. Among the *EiRabX* isotype genes, three genes were up-regulated at later time points, one gene was up-regulated at early time points, while three other *EiRabX* isotype genes were intermittently modulated during the entire encystation process. Variation in the expression pattern of *E. invadens* specific *RabZ* isotype genes was also observed.

Three *E. histolytica* Rabs were previously suggested to be involved in encystation. A gene encoding for EhRab11A (previously named as EhRab11, and re-designated in reference 26) was up-regulated in a "cyst-like" form formed in a serum-deprived medium [36], while *EhRabM1* and *EhRabN1* genes were found to be highly expressed in recent clinical isolates that retained encystation ability, compared to laboratory strain, HM-1 [12]. Up-regulation of *EhRab7D* gene of an avirulent HM-1 strain was reported previously [57], but this gene was also shown to be down-regulated in recent clinical isolates [12]. Our transcriptome data showed that among two Rab subfamily (Rab7 and RabN), *EiRab7D* gene expression was up-regulated at 2 to 120 h of encystation while up-regulation of *EiRab7I* gene expression started earlier (0.5 h) and remained up-regulated up to 48 h of encystation. *EiRabN1* gene expression was upregulated at the 120 h of encystation (Figure 3).

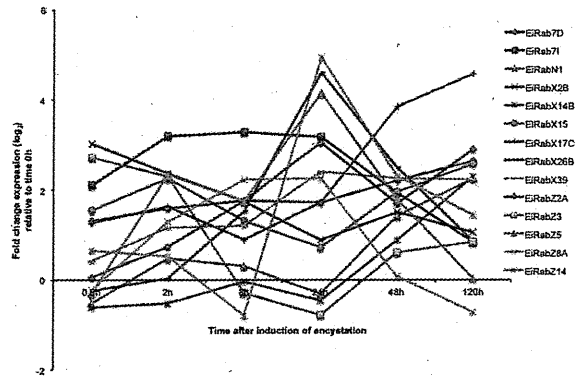

Figure 3. Modulation of the transcripts of 14 *E. invadens* Rab genes during encystation (0.5-120 h). Values are expressed as $\log_2$ fold change of expression relative to time 0 h. Gene IDs: EiRab7D, EIN_133760; EiRab7I, EIN_196420; EiRabN1, EIN_136950; EiRabX2B, EIN_099000; EiRabX14B, EIN_147580; EiRabX15, EIN_238750; EiRabX17C, EIN_107380; EiRabX26B, EIN_060100; EiRabX39, EIN_238590; EiRabZ2A, EIN_289320; EiRabZ3, EIN_192430; EiRabZ5, EIN_039070; EiRabZ8A, EIN_270650; EiRabZ14, EIN_061010.

doi: 10.1371/journal.pone.0074840.g003

H: Cyst wall components

The major components of *E. invadens* cyst wall are the Jacob, Jessie lectins, and chitinase [58]. It has been proposed that these components are assembled in the cyst wall in a "wattle and daub" model, in which Jacob lectins form the wattle, chitinases cross-link the microfibrils, and Jessie lectins form the mortar or daub [59]. Chitin deacetylase acts by cleaving chitin to form chitosan on the surface of the cyst wall [47]. Based on our transcriptomic data (Figure 4), the expression patterns of each lectin and chitin subtype varied. Two genes encoding for EiJacob 1 (EIN_050710_s_at) and 4 (EIN_294450_at) were up-regulated, but the upregulation was not statistically significant. However, expression of *EiJacob1* gene increased at 0.2-120 h, while expression of *EiJacob4* gene increased from 0.5 to 48 h (Table S1), expression of genes encoding EiJacob 2, 3, and chitin synthases were up-regulated at 2 h, followed by those encoding EiJacob 5, 6, 7, chitin deacetylase 2, and chitinase 2 at 8 h. Expression of *EiJessie1c* gene was up-regulated at 8-48 h. Expression of *EiJessie3a, 3b*, and *chitinase 1* genes were upregulated at 24 h (Figure 4). Chitinase 3 was constitutively expressed. Therefore, the expression profiles of these components do not support the proposed "wattle and daub" model, and may suggest post-transcriptional regulation of these proteins.

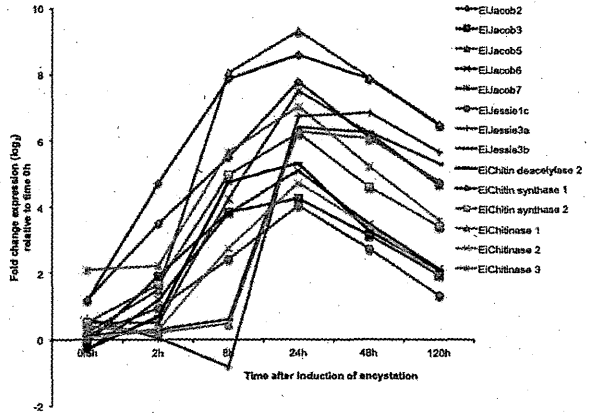

Figure 4. Modulation of the transcript level of the *E. invadens* cyst wall components during encystation (0.5-120 h). Values are expressed as $\log_2$ fold change of expression relative to time 0 h. Gene IDs: EiJacob 2, EIN_137570; EiJacob 3, EIN_016240; EiJacob 5, EIN_104770; EiJacob 6, EIN_015880; EiJacob 7, EIN_186850; EiJessie 1c, EIN_243430; EiJessie 3a, EIN_040990; EiJessie 3b, EIN_058620; EiChitinase 1, EIN_239240; Eichitinase 2, EIN_053310; Eichitinase 3, EIN_059870; EiChitin deacetylase 2, EIN_058630; EiChitin synthase 1, EIN_040930; EiChitin synthase 2, EIN_168780.

doi: 10.1371/journal.pone.0074840.g004

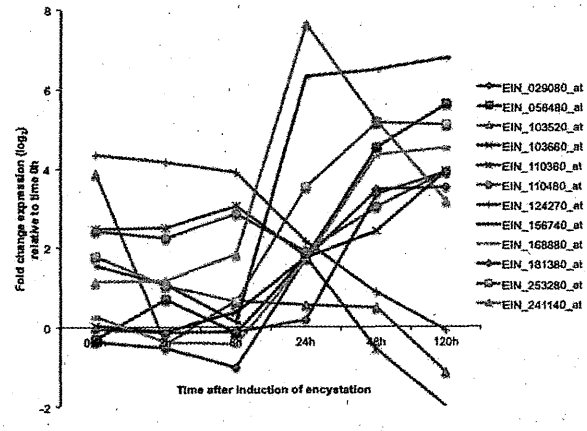

Figure 5. Modulation of the transcript level of the *E. invadens* Myb transcription factors during encystation (0.5-120 h). Values are expressed as $\log_2$ fold change of expression relative to time 0 h after induction of encystation.

doi: 10.1371/journal.pone.0074840.g005

I. Myb transcription factors with R2R3 and $^{T}/_{S}$HAQK$^{Y}/_{F}$ motifs

The Myb family of transcription factors is essential in regulating cell differentiation, cell proliferation, and cell cycle [60]. Recent *in silico* analysis of the *E. histolytica* genome showed 34 proteins with Myb DNA-binding domains [61]. A gene encoding for one of these Mybs with a $^{T}/_{S}$HAQK$^{Y}/_{F}$ motif was shown to be developmentally regulated [12]. It has also been shown that this Myb transcription factor regulates expression of a subset of stage-specific genes in *E. histolytica* [23]. Using the Pathema *Entamoeba* genome database, we searched for *E. invadens* Mybs, and identified a total of 37 *E. invadens* Myb genes encoding Myb proteins with R2R3 and $^{T}/_{S}$HAQK$^{Y}/_{F}$ conserved motifs. Twenty-eight putative *E. invadens* Myb proteins (25 annotated and 3 hypothetical proteins) possess conserved R2R3 repeats, eleven of these were differentially expressed (Figure 5). The $^{T}/_{S}$HAQK$^{Y}/_{F}$ motif was found in 9 hypothetical proteins; and only one gene (EIN_241140_at) of them was up-regulated during encystation (Figure 5). The expression profiles of most of these *Myb* genes were different, which is consistent with a notion that each Myb transcription factor controls expression of specific subsets of genes on a specific phase of encystation, as previously suggested [23].

J: Cysteine proteases

Fifty cysteine proteases (CPs) have been identified in the *E. histolytica* genome [24]. Ten of these CPs were detected in trophozoites, most of which appear to be linked with virulence [3,26,62–65]. However, the role of CPs in encystation has not been elucidated. Recently, 8 CP genes have shown to be differentially expressed in cysts using xenic *E. histolytica* clinical isolates [12].

Cysteine proteases in *E. invadens* were previously identified and annotated [29]. We grouped 64 *E. invadens* CPs into three categories: cyst specific CPs (11 EiCPs), expression of which increased at 24 to 120 h; trophozoite specific CPs (19 EiCPs), expression of which was higher at 0 to 8 h of encystation compared to 24 to 120 h; and constitutively expressed CPs (34 EiCPs) (Figure 6A). Among the modulated CPs (Figure 6B), six belongs to C1 papain superfamily clades A and B (EiCP-A2c, EiCP-A3e, EiCP-BA, EiCP-BB, EiCP-B6, and EiCP-B9), one calpain-like protease (EiCalp2b), two ubiquitin carboxy-terminal hydrolases (EiUCHa and EiUCHc), and one Ulp protease (EiUlpC). Ulp proteases are a group of peptidases that control the function of SUMO. Expression of *EiCP-A2c* and *EiCP-BB* genes was up-regulated at early time points, while that of *EiCP-B9* and *EiUCHa* genes were up-regulated at 24 and 120 h, respectively. Six EiCPs were up-regulated at 24 h or later of encystation. The most striking result was the 61-fold up-regulation of *EiCP-BA* transcript at 24h of encystation. The closest homolog of EiCP-BA is EhCP-B6, although EiCP-BA has a transmembrane domain and an ERFNIN motif similar with a cathepsin L-like enzyme [3,65]. Additionally, expression levels of *EiCP-B6* and *EiCP-UCHa* genes, which were not expressed at 0-0.5 h of encystation, dramatically increased by 99 and 68 fold at 24 h, respectively. *E. histolytica* genes homologous to *EiCP-A3e* and *EiCP-B9* genes in were also up-regulated in cysts [12]. Further studies on the cellular localization of these newly-identified stage-regulated CPs are required to determine whether *E. invadens* CPs may be involved in encystation, as demonstrated in *Giardia lamblia*, where cysteine protease 2 was co-transported with cyst wall

protein in encystation-specific vesicles and plays a central role during encystation [17].

In addition, the EhCP-B9/EhCP112 homolog in *E. invadens* [29] was shown to be accumulated near the cyst wall of immature cysts and further evenly distributed in the cytosol of mature cysts. Transcription of EiCP-B9 also increased 126 fold at 24 h of encystation, which coincide the initiation of the cyst wall formation [18].

K: Heat shock proteins

Microarray analysis of heat shock induced *E. histolytica* showed up-regulation of Gal/GalNAc lectin, cysteine proteases, and heat shock proteins such as Hsp70 (EHI_197860, EHI_199590) and Hsp90 (EHI_102270, EHI_163480) [66]. Exposure of *E. invadens* trophozoites to similar conditions also increased the mRNA expression of *BiP* gene (GenBank AAF64243.1) and was suggested to be partially linked with encystation based on an increased expression of *Jacob* and *chitinase* genes in *E. invadens*, although heat shock per se did not result in the formation of the cyst wall [67]. The closest homolog of this *E. invadens BiP* gene on our array is luminal binding protein 4 precursor (EIN_105260, 58% identity), which also contains the ER-retention signal motif (KDEL) required for its proper targeting to the endoplasmic reticulum [67,68]. However, the mRNA level of EIN_105260 was unchanged at 0-24 h and only slightly increased (1.4 fold) at 120 h of encystation (Table S1). Our transcriptome data did not support the premise that the expression of *BiP* and *chitinase* genes is linked or coincides in *E. invadens*. Up-regulation of *chitinase 1* gene expression peaked at 24 h (78-fold up-regulated). Expression of *chitinase 2* genes increased by 7 fold at as early as 8 h, and peaked at 24 h (26 fold up-regulation) of encystation. In contrast, *chitinase 3* gene was constitutively expressed (Figure 4).

Conclusions

Our transcriptomic analysis of *E. invadens* revealed global changes of gene expression during encystation, and should help to identify key regulatory genes that are essential for the process. Further studies on individual genes and their encoded products that are modulated during encystation may lead to the discovery of targets for the development of new chemotherapeutics that interfere with stage conversion of the parasite.

Supporting Information

Figure S1. Correlation between two biological replicates. The correlation levels of transcripts in DNA microarray analysis between first and second biological replicates at different time points during encystation is shown. The Pearson correlation coefficients were calculated using Excel (2011) workbook.
(TIF)

Table S1. List of all probe sets representing *E. invadens* open reading frames. The *E. invadens* probeset ID, fold change and regulation relative to time 0 h (trophozoite stage), average hybridization signal intensities (raw expression data) of five arrays at each time point, normalized $\log_2$ transformed value, common names, gene ID and predicted GO function are shown.
(XLSX)

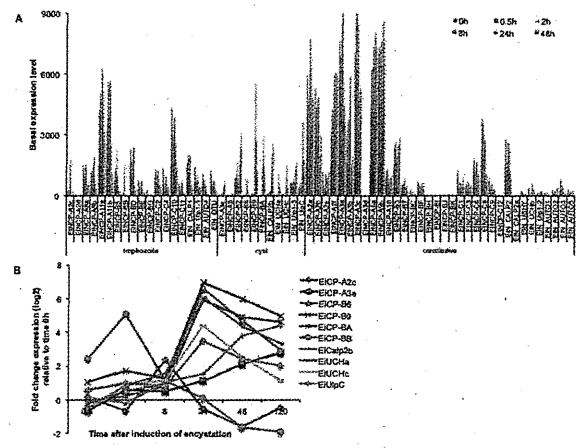

Figure 6. Modulation of the transcript level of the *E. invadens* cysteine proteases during encystation (0.5-120 h). (**A**) Sixty four CPs were grouped into trophozoite-, cyst-predominant, and constitutively expressed CPs based on the transcriptome profiles. **B**) Line graphs showing the fold change expression ($\log_2$) relative to time 0h of ten EiCPs whose expression were significantly modulated during encystation. Gene IDs: EiCP-A2c, EIN_168460; EiCP-A3e, EIN_192250; EiCP-B6, EIN_292720; EiCP-B9, EIN_152250; EiCP-BA, EIN_184830; EiCP-BB, EIN_199850; EiCalp2b, EIN_187000; EiUCHa, EIN_243050; EiUCHc, EIN_107760; EiUlpC, EIN_200450.
doi: 10.1371/journal.pone.0074840.g006

Table S2. Normalized transcriptome data of genes present at least one time points during encystation. The *E. invadens* probe set ID, p-value and corrected p-value of ANOVA, post-hoc test, fold change and regulation relative to time 0 h (trophozoite stage), normalized expression levels in $\log_2$ scale, Pathema/AmoebaDB gene ID, common names, predicted GO function of two biological replicate are shown.
(XLSX)

Table S3. List of genes which were up-regulated ≥ 3 fold at one or more time points during encystation. The *E. invadens* probeset ID, fold change and regulation relative to time 0 h (trophozoite stage), average hybridization signal intensities (raw expression data) of five arrays at each time point, normalized $\log_2$ transformed value, common names, gene id and predicted GO function are shown.
(XLSX)

Table S4. List of genes which were up-regulated ≥ 3 fold at 0.5 and 2 h of encystation. The *E. invadens* probeset ID, fold change and regulation relative to time 0 h (trophozoite stage), average hybridization signal intensities (raw expression data) of five arrays at each time point, normalized $\log_2$ transformed value, common names, gene ID and predicted GO function are shown.
(XLSX)

Table S5. List of genes which were up-regulated ≥ 3 at 8 h of encystation. The *E. invadens* probeset ID, fold change and regulation relative to time 0h (trophozoite stage), average hybridization signal intensities (raw expression data) of five arrays at each time point, normalized $\log_2$ transformed value, common names, gene ID and predicted GO function are shown.
(XLSX)

Table S6. List of genes which were up-regulated ≥ 3 fold at 24 h of encystation. The *E. invadens* probeset ID, fold change and regulation relative to time 0 h (trophozoite stage), average hybridization signal intensities (raw expression data) of five arrays at each time point, normalized $\log_2$ transformed value, common names, gene ID and predicted GO function are shown.
(XLSX)

Table S7. List of genes which were up-regulated ≥ 3 fold at 48 and 120h of encystation. The *E. invadens* probeset ID, fold change and regulation relative to time 0h (trophozoite stage), average hybridization signal intensities (raw expression data) of five arrays at each time point, normalized $\log_2$ transformed value, common names, gene ID and predicted GO function are shown.
(XLSX)

Table S8. List of *E. invadens* transmembrane kinases genes induced ≥ 3 fold at one or more time points during encystation. The *E. invadens* probeset ID, annotation, closest homolog in *E. histolytica* TMKs (number and group), expression in previous studies [12,20,43] predicted number of transmembrane domains (TMHMM) and conserved sequence motifs [43] are shown.
(XLSX)

Author Contributions

Conceived and designed the experiments: AE GJ KN TN. Performed the experiments: AE GJ. Analyzed the data: AE GJ KN TN. Contributed reagents/materials/analysis tools: AE KN EC TN. Wrote the manuscript: AE GJ TN.

References

1. Stanley SL (2003) Amebiasis. Lancet 361: 1025-1034. doi:10.1016/S0140-6736(03)12830-9. PubMed: 12660071.
2. Nozaki T, Kobayashi S, Takeuchi T, Haghighi A (2005) The diversity of clinical isolates of *Entamoeba histolytica* in Japan. Arch Med Res 37: 276-278.
3. Clark CG, Alsmark UC, Tazreiter M, Saito-Nakano Y, Ali V et al. (2007) Structure and content of the *Entamoeba histolytica* genome. Adv Parasitol 65: 51–190. doi:10.1016/S0065-308X(07)65002-7. PubMed: 18063096.
4. Eichinger D (1997) Encystation of *Entamoeba* parasites. Bioessays 19: 633-638. doi:10.1002/bies.950190714. PubMed: 9230696.
5. Donaldson M, Heyneman D, Dempster R, Garcia L (1975) Epizootic of fatal amebiasis among exhibited snakes: epidemiologic, pathologic, and chemotherapeutic considerations. Am J Vet Res 36: 807-817. PubMed: 1147335.
6. Kojimoto A, Uchida K, Horii Y, Okumura S, Yamaguch R et al. (2001) Amebiasis in four ball pythons, Python reginus. J Vet Med Sci 63: 1365-1368. doi:10.1292/jvms.63.1365. PubMed: 11789622.
7. Chia MY, Jeng CR, Hsiao SH, Lee AH, Chen CY et al. (2009) *Entamoeba invadens* myositis in a common water monitor lizard (Varanus salvator). Vet Pathol 46: 673–676. doi:10.1354/vp.08-VP-0224-P-CR. PubMed: 19276058.
8. Sanchez L, Enea V, Eichinger D (1994) Identification of a developmentally regulated transcript expressed during encystation of *Entamoeba invadens*. Mol Biochem Parasitol 67: 125–135. doi:10.1016/0166-6851(94)90102-3. PubMed: 7838173.
9. Gonzalez J, Bai G, Frevert U, Corey EJ, Eichinger D (1999) Proteasome-dependent cyst formation and stage-specific ubiquitin mRNA accumulation in *Entamoeba invadens*. Eur J Biochem 264: 897-904. doi:10.1046/j.1432-1327.1999.00682.x. PubMed: 10491138.
10. Coppi A, Eichinger D (1999) Regulation of *Entamoeba invadens* encystation and gene expression with galactose and N-acetylglucosamine. Mol Biochem Parasitol 102: 67-77. doi:10.1016/S0166-6851(99)00085-7. PubMed: 10477177.
11. Eichinger D (2001) Encystation in parasitic protozoa. Curr Opin Microbiol 4: 421-426. doi:10.1016/S1369-5274(00)00229-0. PubMed: 11495805.
12. Ehrenkaufer GM, Haque R, Hackney JA, Eichinger DJ, Singh U (2007) Identification of developmentally regulated genes in *Entamoeba histolytica*: insights into mechanisms of stage conversion in a protozoan parasite. Cell Microbiol 9: 1426–1444. doi:10.1111/j.1462-5822.2006.00882.x. PubMed: 17250591.
13. Makioka A, Kumagai M, Ohtomo H, Kobayashi S, Takeuchi T (2000) *Entamoeba invadens*: Protein kinase C inhibitors block the growth and encystation. Exp Parasitol 95: 288-290. doi:10.1006/expr.2000.4538. PubMed: 11038313.
14. Makioka A, Kumagai M, Ohtomo H, Kobayashi S, Takeuchi T (2001) Inhibition of encystation of *Entamoeba invadens* by wortmannin. Parasitol Res 87: 371-375. doi:10.1007/s004360000339. PubMed: 11403379.
15. Byers J, Faigle W, Eichinger D (2005) Colonic short-chain fatty acids inhibit encystation of *Entamoeba invadens*. Cell Microbiol 7: 269-279. PubMed: 15659070.
16. Bulik DA, va Ophem P, Manning JM, Shen Z, Newburg DS et al. (2000) UDP-N-acetylglucosamine pyrophosphorylase, a key enzyme in encysting *Giardia*, is allosterically regulated. J Biol Chem 275: 14722-14728. PubMed: 10799561.
17. DuBois KN, Abodeely M, Sakanari J, Craik CS, Lee M et al. (2008) Identification of the major cysteine protease of *Giardia* and its role in encystation. J Biol Chem 283: 18024–18031. doi:10.1074/jbc.M802133200. PubMed: 18445589.
18. Ebert F, Bachmann A, Nakada-Tsukui K, Hennings I, Drescher B et al. (2008) An *Entamoeba* cysteine peptidase specifically expressed during encystation. Parasitol Int 57: 521–524. PubMed: 18723116.
19. Kriebel PW, Parent CA (2004) Adenylyl cyclase expression and regulation during the differentiation of *Dictyostelium discoideum*. IUBMB Life 56: 541–546. doi:10.1080/15216540400013887. PubMed: 15590560.
20. Gilchrist CA, Houpt E, Trapaidze N, Fei Z, Crasta O et al. (2006) Impact of intestinal colonization and invasion on the *Entamoeba histolytica* transcriptome. Mol Biochem Parasitol 147: 163–176. doi:10.1016/j.molbiopara.2006.02.007. PubMed: 16569449.
21. MacFarlane RC, Singh U (2006) Identification of differentially expressed genes in virulent and nonvirulent *Entamoeba* species: potential implications for amebic pathogenesis. Infect Immun 74: 340-351. doi:10.1128/IAI.74.1.340-351.2006. PubMed: 16368989.
22. Vicente JB, Ehrenkaufer GM, Saraiva LM, Teixeira M, Singh U (2009) *Entamoeba histolytica* modulates a complex repertoire of novel genes

in response to oxidative and nitrosative stresses: implications for amebic pathogenesis. Cell Microbiol 11: 51-69. doi:10.1111/j.1462-5822.2008.01236.x. PubMed: 18778413.
23. Ehrenkaufer GM, Hackney JA, Singh U (2009) A developmentally regulated Myb domain protein regulates expression of a subset of stage-specific genes in *Entamoeba histolytica*. Cell Microbiol 11: 898-910. doi:10.1111/j.1462-5822.2009.01300.x. PubMed: 19239479.
24. González-Salazar F, Viader-Salvadó JM, Martínez-Rodríguez HG, Campos-Góngora E, Mata-Cárdenas BD et al. (2000) Identification of seven chemical factors that favor high-quality *Entamoeba histolytica* cyst-like structure formation under axenic conditions. Arch Med Res 31 (Suppl): 192–193. doi:10.1016/S0188-4409(00)00193-4. PubMed: 11070279.
25. Barrón-González MP, Villarreal-Treviño L, Verduzco-Martínez JA, Mata-Cárdenas BD, Morales-Vallarta MR (2005) *Entamoeba invadens*: in vitro axenic encystation with a serum substitute. Exp Parasitol 110: 318–321. doi:10.1016/j.exppara.2005.03.021. PubMed: 15955331.
26. Tillack M, Biller L, Irmer H, Freitas M, Gomes MA et al. (2007) The *Entamoeba histolytica* genome: primary structure and expression of proteolytic enzymes. BMC Genomics 8: 170. doi: 10.1186/1471-2164-8-170. PubMed: 17567921.
27. Kumar S, Nei M, Dudley J, Tamura K (2008) MEGA: A biologist-centric software for evolutionary analysis of DNA and protein sequences. Brief Bioinform 9: 299-306. doi:10.1093/bib/bbn017. PubMed: 18417537.
28. Nakada-Tsukui K, Saito-Nakano Y, Husain A, Nozaki T (2010) Conservation and function of Rab small GTPases in *Entamoeba*: annotation of E. invadens Rab and its use for the understanding of *Entamoeba* biology. Exp Parasitol 126: 337-347. doi:10.1016/j.exppara.2010.04.014. PubMed: 20434444.
29. Nakada-Tsukui K, Nozaki T (2010) Genomic and post-genomic approaches to understand the pathogenesis of the enteric protozoan parasite *Entamoeba histolytica*. In: P FratamicoY LiuS Kathariou. Genomes of Food and Waterborne Pathogens. Washington, DC: ASM Press. pp 321-341.
30. Wang Z, Samuelson J, Clark CG, Eichinger D, Paul J et al. (2003) Gene discovery in the *Entamoeba invadens* genome. Mol Biochem Parasitol 129: 23–31. doi:10.1016/S0166-6851(03)00073-2. PubMed: 12798503.
31. Lorenzi HA, Puiu D, Miller JR, Brinkac LM, Amedeo P et al. (2010) New assembly, reannotation and analysis of the *Entamoeba histolytica* genome reveal new genomic features and protein content information. PLOS Negl Trop Dis 4(6): e716. doi:10.1371/journal.pntd.0000716. PubMed: 20559563.
32. Ikegami A, Honma K, Sharma A, Kuramitsu HK (2004) Multiple functions of the leucine-rich repeat protein LrrA of *Treponema denticola*. Infect Immun 72: 4619–4627. doi:10.1128/IAI.72.8.4619-4627.2004. PubMed: 15271922.
33. Inagaki S, Onishi S, Kuramitsu HK, Sharma A (2006) *Porphyromonas gingivalis* vesicles enhance attachment, and the leucine-rich repeat BspA protein is required for invasion of epithelial cells by "Tannerella forsythiae". Infect Immun 74: 5023-5028. doi:10.1128/IAI.00062-06. PubMed: 16926393.
34. Davis PH, Zhang Z, Chen M, Zhang X, Chakraborty S et al. (2006) Identification of a family of BspA like surface proteins of *Entamoeba histolytica* with novel leucine rich repeats. Mol Biochem Parasitol 145: 111–116. doi:10.1016/j.molbiopara.2005.08.017. PubMed: 16199101.
35. Noël CJ, Diaz N, Sicheritz-Ponten T, Safarikova L, Tachezy J et al. (2010) *Trichomonas vaginalis* vast BspA-like gene family: evidence for functional diversity from structural organisation and transcriptomics. BMC Genomics 11: 99. doi:10.1186/1471-2164-11-99. PubMed: 20144183.
36. McGugan GC, Temesvari LA (2003) Characterization of a Rab11-like GTPase, EhRab11 of *Entamoeba histolytica*. Mol Biochem Parasitol 129: 137–146. doi:10.1016/S0166-6851(03)00115-4. PubMed: 12850258.
37. Hon CC, Nakada-Tsukui K, Nozaki T, Guillen N (2010) Dissecting the actin skeleton from a genomic prespective. In: CG ClarkPJ JohnsonRD Adam. Anaerobic Parasitic Protozoa Genomics and Molecular Biology. Norfolk, UK: Caister Academic Press. pp 81-155.
38. Makioka A, Kumagai M, Ohtomo H, Kobayashi S, Takeuchi T (2000) Effect of cytochalasin D on the growth, encystation, and multinucleation of *Entamoeba invadens*. Parasitol Res 86: 599-602. doi:10.1007/PL00008536. PubMed: 10935912.
39. Picazarri K, Nakada-Tsukui K, Nozaki T (2008) Autophagy during proliferation and encystation in the protozoan parasite *Entamoeba invadens*. Infect Immun 76: 278–288. doi:10.1128/IAI.00636-07. PubMed: 17923513.
40. Makioka A, Kumagai M, Kobayashi S, Takeuchi T (2003) Involvement of signaling through protein kinase C and phosphatidylinositol 3-kinase in the excystation and metacystic development of *Entamoeba invadens*. Parasitol Res 91: 204–208. doi:10.1007/s00436-003-0955-x. PubMed: 12923632.
41. Nakada-Tsukui K, Okada H, Mitra BN, Nozaki T (2009) Phosphatidylinositol-phosphates mediate cytoskeletal reorganization during phagocytosis via a unique modular protein consisting of RhoGEF/DH and FYVE domains in the parasitic protozoon *Entamoeba histolytica*. Cell Microbiol 11: 1471–1491. doi:10.1111/j.1462-5822.2009.01341.x. PubMed: 19496789.
42. Boettner DR, Huston CD, Linford AS, Buss SN, Houpt E (2008) *Entamoeba histolytica* phagocytosis of human erythrocytes involves PATMK, a member of the transmembrane kinase family. PLOS Pathog 4(1): e8. doi:10.1371/journal.ppat.0040008. PubMed: 18208324.
43. Buss SN, Hamano S, Vidrich A, Evans C, Zhang Y et al. (2010) Members of the *Entamoeba histolytica* transmembrane kinase family play non-redundant roles in growth and phagocytosis. Int J Parasitol 40: 833-843. doi:10.1016/j.ijpara.2009.12.007. PubMed: 20083116.
44. Beck DL, Boettner DR, Dragulev B, Ready K, Nozaki T et al. (2005) Identification and gene expression analysis of a large family of transmembrane kinases related to the Gal/GalNAc lectin in *Entamoeba histolytica*. Eukaryot Cell 4: 722-732. doi:10.1128/EC.4.4.722-732.2005. PubMed: 15821132.
45. Shiozaki K, Russell P (1994) Cellular function of protein phosphatase 2C in yeast. Cell Mol Biol Res 40: 241-243. PubMed: 7874201.
46. Jeelani G, Sato D, Husain A, Escueta-de Cadiz A, Sugimoto M, Soga T, Suematsu M, Nozaki T (2012) Metabolic profiling of the protozoan parasite *Entamoeba invadens* revealed activation of unpredicted pathway during encystation. PLOS ONE 7: e37740. doi:10.1371/journal.pone.0037740. PubMed: 22662204.
47. Das S, Van Dellen K, Bulik D, Magnelli P, Cui J et al. (2006) The cyst wall of *Entamoeba invadens* contains chitosan (deacetylated chitin). Mol Biochem Parasitol 148: 86–92. PubMed: 16621070.
48. Lopez AB, Sener K, Jarroll EL, Van Keulen H (2003) Transcription regulation is demonstrated for five key enzymes in Giardia intestinalis cyst wall polysaccharide biosynthesis. Mol Biochem Parasitol 128: 51-57. doi:10.1016/S0166-6851(03)00049-5. PubMed: 12706796.
49. Gallego E, Alvarado M, Wasserman M (2007) Identification and expression of the protein ubiquitination system in *Giardia intestinalis*. Parasitol Res 101: 1-7. doi:10.1007/s00436-007-0605-9. PubMed: 17252268.
50. Ulrich HD (2005) Mutual interactions between the SUMO and ubiquitin systems: A plea of no contest. Trends Cell Biol 15: 525–532. doi: 10.1016/j.tcb.2005.08.002. PubMed: 16125934.
51. Pao SS, Paulsen IT, Saier MH Jr (1998) Major Facilitator Superfamily. Microbiol Mol Biol Rev 62: 1-34. PubMed: 9529885.
52. Campos-Góngora E, Viader-Salvadó JM, Martínez-Rodríguez HM, Zuñiga-Charles MA (2000) Mg, Mn, and Co Ions enhance the formation of *Entamoeba histolytica* cyst-Like structures resistant to sodium dodecyl sulfate. Arch Med Res 31: 162–168. doi:10.1016/S0188-4409(00)00054-0. PubMed: 10880721.
53. González-Salazar F, Viader-Salvadó JM, Martínez-Rodríguez HG, Campos-Góngora E, Mata-Cárdenas BD et al. (2000) Identification of seven chemical factors that favor high-quality *Entamoeba histolytica* cyst-like structure formation under axenic conditions. Arch Med Res 31: S192-S193. doi:10.1016/S0188-4409(00)00193-4. PubMed: 11070279.
54. Das S, Gillin FD (1991) Chitin synthase in encysting *Entamoeba invadens*. Biochem J 20: 641-647. PubMed: 1764027.
55. Said-Fernández S, Campos-Góngora E, González-Salazar F, Martínez-Rodríguez HG, Vargas-Villarreal J (2001) Mg^{2+}, Mn^{2+}, and Co^{2+} stimulate *Entamoeba histolytica* to produce chitin-like material. J Parasitol 87: 919-923. doi: 10.1645/0022-3395(2001)087[0919:MMACSE]2.0.CO;2. PubMed: 11534662.
56. Abeijon C, Mandon EC, Hirschberg CB (1997) Transporters of nucleotide sugars, nucleotide sulfate and ATP in the Golgi apparatus. Trends Biochem Sci 22: 203-207. doi:10.1016/S0968-0004(97)01053-0. PubMed: 9204706.
57. Biller L, Davis PH, Tillack M, Matthiesen J, Lotter H, Stanley SL, Tannich E, Bruchhaus I (2010) Differences in the transcriptome signatures of two genetically related *Entamoeba histolytica* cell lines derived from the same isolate with different pathogenic properties. BMC Genomics 11: 63. doi:10.1186/1471-2164-11-63. PubMed: 20102605.
58. Van Dellen KL, Chatterjee A, Ratner DM, Magnelli PE, Cipollo JF et al. (2006) Unique posttranslational modifications of chitin-binding lectins of *Entamoeba invadens* cyst walls. Eukaryot Cell 5: 836-848. doi: 10.1128/EC.5.5.836-848.2006. PubMed: 16682461.

59. Chatterjee A, Ghosh SK, Jang K, Bullitt E, Moore L et al. (2009) Evidence for a "wattle and daub" model of the cyst wall of *Entamoeba*. PLOS Pathog 5(7): e1000498.
60. Rosinski JA, Atchley WR (1998) Molecular evolution of the Myb family of transcription factors: evidence for polyphyletic origin. J Mol Evol 46: 74–83. doi:10.1007/PL00006285. PubMed: 9419227.
61. Meneses E, Cárdenas H, Zárate S, Brieba LG, Orozco E et al. (2010) The R2R3 Myb protein family in *Entamoeba histolytica*. Gene 455: 32-42. doi:10.1016/j.gene.2010.02.004. PubMed: 20156532.
62. Que X, Reed SL (2000) Cysteine proteinases and the pathogenesis of amebiasis. Clin Microbiol Rev 13: 196-206. doi:10.1128/CMR.13.2.196-206.2000. PubMed: 10755997.
63. Moncada D, Keller K, Chadee K (2003) *Entamoeba histolytica* cysteine proteinases disrupt the polymeric structure of colonic mucin and alter its protective function. Infect Immun 71: 838–844. doi:10.1128/IAI.71.2.838-844.2003. PubMed: 12540564.
64. Bruchhaus I, Loftus BJ, Hall N, Tannich E (2003) The intestinal protozoan parasite *Entamoeba histolytica* contains 20 cysteine protease genes, of which only a small subset is expressed during in vitro cultivation. Eukaryot Cell 2: 501–509. doi:10.1128/EC.2.3.501-509.2003. PubMed: 12796295.
65. He C, Nora GP, Schneider EL, Kerr ID, Hansell K et al. (2010) A novel *Entamoeba histolytica* cysteine proteinase, EhCP4, is key for invasive amebiasis and a therapeutic target. J Biol Chem 285: 18516–18527.
66. Weber C, Guigon G, Bouchier C, Frangeul L, Moreira S et al. (2006) Stress by heat shock induces massive down regulation of genes and allows differential allelic expression of the Gal/GalNAc lectin in *Entamoeba histolytica*. Eukaryot Cell 5: 871-875. doi:10.1128/EC.5.5.871-875.2006. PubMed: 16682464.
67. Field J, Van Dellen K, Ghosh SK, Samuelson J (2000) Responses of *Entamoeba invadens* to heat shock and encystation are related. J Eukaryot Microbiol 47: 511-514. doi:10.1111/j.1550-7408.2000.tb00083.x. PubMed: 11001149.
68. Ghosh SK, Field J, Frisardi M, Rosenthal B, Mai Z et al. (1999) Chitinase secretion by encysting *Entamoeba invadens* and transfected *Entamoeba histolytica* trophozoites: localization of secretory vesicles, endoplasmic reticulum and golgi apparatus. Infect Immun 67: 3073-3081. PubMed: 10338523.

IAI
Journals.ASM.org

Cysteine Protease-Binding Protein Family 6 Mediates the Trafficking of Amylases to Phagosomes in the Enteric Protozoan *Entamoeba histolytica*

Atsushi Furukawa,[a,b]* Kumiko Nakada-Tsukui,[a] Tomoyoshi Nozaki[a,c]

Department of Parasitology, National Institute of Infectious Diseases, Toyama, Tokyo, Japan[a]; Department of Parasitology, Gunma University Graduate School of Medicine, Maebashi, Japan[b]; Graduate School of Life and Environmental Sciences, University of Tsukuba, Tsukuba, Ibaraki, Japan[c]

Phagocytosis plays a pivotal role in nutrient acquisition and evasion from the host defense systems in *Entamoeba histolytica*, the intestinal protozoan parasite that causes amoebiasis. We previously reported that *E. histolytica* possesses a unique class of a hydrolase receptor family, designated the cysteine protease-binding protein family (CPBF), that is involved in trafficking of hydrolases to lysosomes and phagosomes, and we have also reported that CPBF1 and CPBF8 bind to cysteine proteases or β-hexosaminidase α-subunit and lysozymes, respectively. In this study, we showed by immunoprecipitation that CPBF6, one of the most highly expressed CPBF proteins, specifically binds to α-amylase and γ-amylase. We also found that CPBF6 is localized in lysosomes, based on immunofluorescence imaging. Immunoblot and proteome analyses of the isolated phagosomes showed that CPBF6 mediates transport of amylases to phagosomes. We also demonstrated that the carboxyl-terminal cytosolic region of CPBF6 is engaged in the regulation of the trafficking of CPBF6 to phagosomes. Our proteome analysis of phagosomes also revealed new potential phagosomal proteins.

Phagocytosis and phagosome biogenesis play indispensable and pivotal roles in the pathogenesis of *Entamoeba histolytica*. *E. histolytica* trophozoites ingest and digest microorganisms in the large intestine, for the acquisition of nutrients (1), and also host cells (2) during tissue invasion, for the creation of a parasitic niche. Phagocytosis also plays a role in the evasion from host immune systems (3). It has been demonstrated that the levels of *in vitro* and *in vivo* virulence of clinical and laboratory strains correlate well with the ability for phagocytosis (4–7). In addition, phagosomes contain a panel of proteins that have been implicated in pathogenesis, such as cysteine proteases (CPs) (8), amoeba pores (9), and galactose-/*N*-acetylgalactosamine-specific lectin (10, 11). Therefore, an understanding of the molecular mechanisms of phagosome biogenesis and trafficking, together with the characterization of "uncharacterized hypothetical" proteins in phagosomes, should further uncover the links between phagocytosis and pathogenicity.

Recently, the molecular mechanisms of phagocytosis have started to be unveiled. For example, an unconventional myosin, myosin IB, was shown to be involved in cytoskeleton rearrangement during phagocytosis (12). It was also shown that phosphatidylinositol signaling is involved in phagocytosis. The time- and position-specific accumulations of phosphatidylinositol-3-phosphate (PI3P) and phosphatidylinositol (3,4,5)-trisphosphate (PIP3) (13–15) on the phagosomal membrane were demonstrated. Surface Ca^{2+}-binding kinase (C2PK) was shown to be involved in the initiation of phagocytosis (16). C2PK localizes in close proximity to the plasma membrane through phosphatidylserine in the presence of Ca^{2+} and thereby recruits *E. histolytica* CaBP1 (EhCaBP1) and actin to the phagocytic cup during erythrophagocytosis. Conditional suppression of C2PK expression and overexpression of a mutant form demonstrated its role in the initiation of the formation of the phagocytic cup. Surface transmembrane kinase (TMK96) and p21-activated kinase (PAK) also have been shown to play important roles in phagocytosis of human erythrocytes (17, 18). TMK96 was identified in the proteome of isolated phagosomes and plays an important role in the clearance of dead host cells. PAK was shown to be highly concentrated in the nascent pseudopod in motile trophozoites and appears to be a regulatory element controlling pseudopod extension and cell polarity. Overproduction of the carboxyl-terminal kinase domain of PAK causes multiple pseudopod formation and enhanced erythrophagocytosis.

Although the mechanisms of initiation of phagocytosis have been vigorously investigated, it is only recently that scientists have started to understand the fundamental mechanisms of how hydrolases are selectively transported to phagosomes, leading to organelle maturation. Transport and activation of hydrolytic enzymes are tightly regulated. Otherwise, they are deleterious to the cell. In yeast and mammals, trafficking of major hydrolytic enzymes is mediated by the specific cargo receptors mannose-6-phosphate receptor (M6PR) and Vps10/sortilin. M6PR regulates the trafficking of M6P-modified lysosomal hydrolases, including cathepsin L and β-hexosaminidase, while Vps10p/sortilin regulates the trafficking of carboxypeptidase Y in yeast or cathepsin D in mammals. *E. histolytica* appears to lack a Vps10/sortilin ho-

Received 30 August 2012 Returned for modification 4 October 2012
Accepted 10 December 2012
Published ahead of print 18 March 2013
Editor: J. F. Urban, Jr.
Address correspondence to Tomoyoshi Nozaki, nozaki@nih.go.jp.
* Present address: Atsushi Furukawa, Laboratory of Bimolecular Science, Faculty of Pharmaceutical Sciences, Hokkaido University, Japan.
Supplemental material for this article may be found at http://dx.doi.org/10.1128/IAI.00915-12.

doi:10.1128/IAI.00915-12

molog. Furthermore, immuno-affinity pulldown of a putative M6PR (EHI_096320) failed to coprecipitate any cargo protein, suggesting that putative M6PRs are not likely receptors/carriers of lysosomal hydrolases (K. Nakada-Tsukui, unpublished data). We recently discovered a novel class of a single-transmembrane carrier/receptor family, designated the cysteine protease-binding protein family (CPBF), that specifically binds to various lysosomal hydrolytic enzymes and regulates their trafficking in *E. histolytica* (19, 20). CPBF consists of 11 proteins (CPBF1 to -11) with significant mutual identity and structural conservation: the signal peptide at the amino terminus, a single transmembrane domain close to the carboxyl terminus, and the YxxΦ motif at the carboxyl terminus. CPBF1 was initially discovered as a receptor/carrier for one of three major cysteine proteases, EhCP-A5 (20). We further demonstrated that CPBF1 is essential for the processing and lysosomal transport of EhCP-A5. On the other hand, CPBF8 binds to β-hexosaminidase α-subunit and lysozymes and transports them to phagosomes (19). We further showed that repression of CPBF8 by gene silencing decreased degradation of the Gram-positive bacillus *Clostridium perfringens* and *in vitro* cytopathic activity against mammalian cells.

In the present study, we have characterized another member of the most highly expressed CPBF genes among the family, *CPBF6*. We show that CPBF6 is distributed to lysosomes in steady state and transported to phagosomes upon phagocytosis. We have further identified cargo proteins, by affinity immunoprecipitation of CPBF6, followed by liquid chromatography-tandem mass spectrometry (LC-MS/MS) analysis, to be α-amylase and γ-amylase. We also confirmed the role of CPBF6 in phagosomal transport of α-amylase and γ-amylase by repression of CPBF6, based on Western blotting and proteome analyses. In addition, this proteome analysis shows a new potential for phagosomal proteins. Finally, we show that the carboxyl-terminal region of CPBF6 plays a crucial role in phagosomal localization.

MATERIALS AND METHODS

Microorganisms and cultivation. Trophozoites of *E. histolytica* HM-1:IMSS Cl-6 and G3 strains (21, 22) were cultured axenically at 35°C in 13- by 100-mm screw-cap Pyrex glass tubes or 25-cm^2 plastic culture flasks in BI-S-33 medium as previously described (23, 24). Chinese hamster ovary (CHO) cells were grown in F-12 medium (Invitrogen, CA) supplemented with 10% fetal bovine serum on a 10-cm-diameter tissue culture dish (Iwaki, Tokyo, Japan) under 5% CO_2 at 37°C.

Plasmid construction and production of *E. histolytica* transformants. The protein-coding region of *CPBF6* was amplified by PCR from cDNA using the sense and antisense oligonucleotides 5′-GCGAGATCTATGTCAATGAGTTGTCTGACTT-3′ and 5′-CAGCGAGATCTAGAAAGGTCATGATAACCA-3′ (BglII restriction sites are underlined). The amplified PCR product was digested with BglII and ligated into BglII-digested pEhExHA (25), to produce pEhEx-CPBF6-HA. The plasmid to produce the mutant form of CPBF6 that lacks a 43-amino-acid (aa)-long serine-rich region (SRR, aa 815 to 857; SSDSSSSSSPSASSTQPSTSSSAPNPSGESSNNTEDNNGTKIG; pEhEx-CPBF6ΔSRR-HA) was constructed as follows. A DNA fragment was amplified by PCR using pEhEx-CPBF6-HA as a template and the sense and antisense oligonucleotides 5′-TGGATTATTTTTGGTGTTGTTCTCTTCTTG-3′ and 5′-TGGTATTTTTTCAAGTTTCATCAATATTTC-3′. The PCR product was treated with the BKL kit (TaKaRa, Shiga, Japan) and self-ligated to produce pEhEx-CPBF6ΔSRR-HA. The resulting plasmid carries a mutant CPBF6 protein that lacks the SRR. pEhEx-CPBF6Δcytosol-HA, which lacks a 15-aa-long cytosolic carboxyl-terminal region after the transmembrane region, and CPBF6ΔNNGYHDLS-HA, which lacks an 8-aa-long cytosolic carboxyl-terminal region, were constructed as follows. The protein-coding region of CPBF6Δcytosol and CPBF6ΔNNGYHDLS were amplified by PCR by using the oligonucleotides 5′-GCGAGATCTATGTCAATGAGTTGTCTGACT-3′ and 5′-GCGAGATCTTATGAAACCAATAATAAAGGC-3′ (for CPBF6Δcytosol) and 5′-GGAAGATCTATGTCAATGAGTTGTCTGACT-3′ and 5′-GGAAGATCTCTTTTTACGATATATTATGAA-3′ (for CPBF6ΔNNGYHDLS) (BglII restriction sites are underlined). respectively. The amplified PCR products were digested with BglII and ligated into BglII-digested pEhExHA to produce pEhEx-CPBF6Δcytosol-HA and CPBF6ΔNNGYHDLS-HA, respectively. The transformants that expressed full-length or truncated forms of CPBF6-HA were established by transfection of the wild-type HM1:IMSS Cl6 strain with pEhEx-CPBF6-HA, pEhEx-CPBF6ΔSRR-HA, pEhEx-CPBF6Δcytosol-HA, or CPBF6ΔNNGYHDLS-HA by liposome-mediated transfection, as previously described (26). For gene silencing of *CPBF6*, the 420-bp-long 5′ end of the CPBF6 protein-coding region was amplified by PCR from cDNA using the oligonucleotides 5′-CGCAGGCCTATGTCAATGAGTTGTCTGACT-3′ and 5′-GCAGAGCTCATAAGCACCAGGGGCAGAATA-3′ (StuI and SacI restriction sites are underlined). The PCR-amplified DNA fragment was digested with StuI and SacI and ligated into StuI- and SacI-digested pSAP2-Gunma, to produce pSAP2-CPBF6. The *CPBF6* gene-silenced strain was established by transfection of the G3 strain with pSAP2-CPBF6 as described above. We also established a control strain by transfection of the G3 strain with pSAP2-Gunma.

Antibodies. Anti-α-amylase and anti-γ-amylase antibodies were raised against a mixture of the peptides DIPLEEFDRLKSKG (aa 45 to 58) and GAHFVENHDENRAV (aa 319 to 332) for α-amylase and RIKKHLNKIRSDLT (aa 547 to 560) and LADEIDGHKSLTAN (aa 607 to 620) for γ-amylase. Pyridine nucleotide transhydrogenase (EhPNT) antibody was previously described (27). Anti-hemagglutinin (HA) 11MO mouse monoclonal antibody was purchased from Berkeley Antibody (Berkeley, CA). Alexa Fluor anti-mouse and anti-rabbit IgG and horseradish peroxidase-conjugated goat anti-mouse and anti-rabbit IgG were purchased from Invitrogen.

Immunofluorescene assay. For the staining of lysosomes, amoebae were incubated in the BI-S-33 medium containing LysoTracker Red DND-99 (Invitrogen; diluted 1:500) at 35°C. CHO cells grown in F-12 medium supplemented with 10% fetal bovine serum were incubated with 10 μM CellTracker Blue (Invitrogen) at 37°C for 1 h. After washing with BI-S-33 medium three times, CellTracker-labeled CHO cells were added to the 8-mm-diameter wells of an 8-well glass slide (Thermo Scientific, Rockford, IL) containing 5×10^4 *E. histolytica* trophozoites, and the mixture was further incubated at 35°C in the BI-S-33 medium. After incubation, cells were fixed with 3.7% paraformaldehyde–phosphate-buffered saline (PBS) for 10 min and permeabilized with 0.2% saponin–PBS for 10 min at ambient temperature. The cells were then allowed to react with anti-HA 11MO mouse monoclonal antibody (diluted 1:1,000) and Alexa Fluor 488 anti-mouse secondary antibody (1:1,000). The samples were examined on a Carl-Zeiss (Thornwood, NY) LSM510 confocal laser-scanning microscope. Images were further analyzed using LSM510 software. We defined CPBF6-positive vacuoles based on criteria described elsewhere (19).

Immunoprecipitation. Approximately 3×10^6 trophozoites of strains expressing CPBF6-HA, CPBF6ΔSRR, CPBF6Δcytosol, or CPBF6ΔNNGYHDLS were lysed in 2 ml of lysis buffer (50 mM Tris-HCl [pH 7.5], 150 mM NaCl, 1% Triton X-100 [Tokyo Kasei, Tokyo, Japan], 0.5 mg/ml E-64 [Sigma-Aldrich, St. Louis, MO], and Complete mini protease inhibitor cocktail [Roche, Basel, Switzerland]). Approximately 10 mg of the lysate was incubated with protein G-Sepharose beads (50 μl of an 80% slurry; Amersham Biosciences, Uppsala, Sweden) in 2 ml of lysis buffer at 4°C for 90 min, and centrifuged at $800 \times g$ at 4°C for 3 min to remove proteins that were nonspecifically bound to the protein G-Sepharose beads. The precleared lysate was mixed with 90 μl of anti-HA antibody conjugated to agarose (50% slurry; Sigma-Aldrich) and incu-

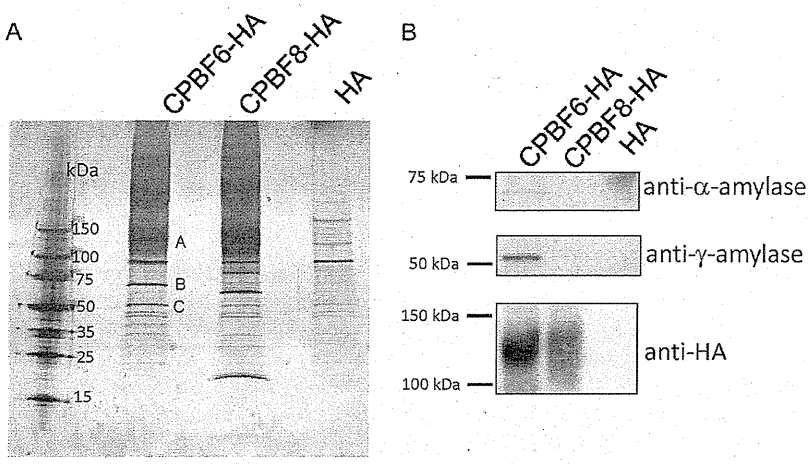

FIG 1 Isolation and identification of CPBF6-binding proteins. Lysates of CPBF6-HA, CPBF8-HA, and control (HA) transformants were mixed with anti-HA-antibody-conjugated agarose, washed, and eluted with HA peptide. The eluates were separated on SDS-PAGE and silver stained (A) or subjected to Western blotting with anti-α-amylase, anti-γ-amylase, and anti-HA antibody (B). Apparent molecular masses of standards are indicated on the left. Three bands excised for protein identification are labeled (A to C).

bated at 4°C for 3.5 h. The agarose beads were collected by centrifugation at 800 × *g* at 4°C for 3 min and washed four times with wash buffer (50 mM Tris-HCl [pH 7.5], 150 mM NaCl, 1% Triton X-100). The agarose beads were then incubated with 180 μl of HA peptide (20 μg/ml) at 4°C overnight to dissociate proteins from the beads. The eluate was applied to SDS-PAGE gels, and silver stained, immunoblotting, activity assays, and protein sequencing were performed.

Protein digestion, LC-MS/MS), and database search for protein identification. For identification of phagosomal proteins, we carried out two different digestion methods for LC-MS/MS analysis. Briefly, for the solution method, a 50-μg equivalent of the protein solution was extracted with 300 μl methanol–75 μl chloroform–225 μl water. After the upper aqueous layer was discarded, 325 μl of methanol was added to the organic phase. The sample was vitiated and centrifuged for 5 min. The pellet was air dried and resuspended in ammonium bicarbonate, reduced, alkylated, and digested with 1 μg trypsin (Promega, Madison, WI) overnight at room temperature. The sample was acidified to 5% with acetic acid and then subjected to LC-MS/MS. For the in-gel digestion method, a 10-μg equivalent of the solution was subjected to SDS-PAGE until the dye front migrated ~1 cm. An approximately 1-cm^2 piece was excised from the gel, transferred to a siliconized tube, and destained in 200 μl of 50% methanol overnight. The gel pieces were dehydrated in acetonitrile, rehydrated in 30 μl of 10 mM dithiothreitol in 0.1 M ammonium bicarbonate, and reduced with dithiothreitol at room temperature for 0.5 h. The dithiothreitol solution was removed and the sample alkylated in 30 μl 50 mM iodoacetamide in 0.1 M ammonium bicarbonate at room temperature for 0.5 h. The reagent was removed, and the gel pieces were dehydrated in 100 μl acetonitrile. The acetonitrile was removed, and the gel pieces were rehydrated in 100 μl 0.1 M ammonium bicarbonate. The pieces were dehydrated in 100 μl acetonitrile, the acetonitrile was removed, and the pieces were completely dried by vacuum centrifugation. The gel pieces were rehydrated in 20 ng/μl trypsin in 50 mM ammonium bicarbonate on ice for 10 min. Any excess enzyme solution was removed, and 20 μl of 50 mM ammonium bicarbonate was added. The sample was digested overnight at 37°C, and the peptides that formed were extracted from the polyacrylamide in two 30-μl aliquots of 50% acetonitrile–5% formic acid. These extracts were combined and evaporated to 15 μl for MS analysis.

The LC-MS/MS system consisted of a Thermo Electron Orbitrap Velos ETD mass spectrometer system with a Protana nanospray ion source interfaced with a self-packed 8-cm by 75-μm (inner diameter) Phenomenex Jupiter 10-μm C_{18} reversed-phase capillary column. Approximately 2-μg equivalents of each sample were injected, and the peptides were eluted from the column with an acetonitrile–0.1 M acetic acid gradient at a flow rate of 0.5 μl/min over 2 h. The nanospray ion source was operated at 2.5 kV. The digest was analyzed using the double-play capability of the instrument, acquiring full scan mass spectra to determine peptide molecular weights and product ion spectra to identify amino acid sequences in sequential scans. This mode of analysis produces approximately 30,000 CAD spectra of ions that range in abundance over several orders of magnitude.

The data were analyzed by database searches using the Sequest search algorithm against the *E. histolytica* genome database at the J. Craig Venter Institute (http://www.jcvi.org/). The identified proteins were considered phagosomal when two unique peptides were detected.

Transcriptomic analysis. Expression analysis was performed by using a custom-made *E. histolytica* array from Affymetrix, Inc. (Santa Clara, CA), as previously described (28–30). Labeled cRNA for hybridization was prepared from 5 μg of total RNA, according to the protocol of the manufacturer. Hybridization and scanning were also performed according to the protocols of the manufacturer. Raw probe intensities were generated by using the GeneChip operating software (GCOS) and a GeneTitan instrument. The averages of triplicate raw probe intensities are reported.

Phagosome purification. Phagosome purification was performed as previously described (19, 31, 32). Briefly, amoebae were incubated with carboxylated latex beads for 1 h, and after brief centrifugation, the cell pellet was resuspended and mechanically homogenized by using a Dounce homogenizer. The phagosomes were isolated by ultracentrifugation on a sucrose gradient.

Enzymatic assay. The amylase assay was performed by using the EnzChek amylase assay kit (Invitrogen). Briefly, the amoeba lysate, culture supernatant, or phagosomal fraction was mixed with 200 μg/ml substrate solution containing BODIPY FL-conjugated DQ starch in 100 μl of 0.1 M morpholinepropanesulfonic acid (MOPS; pH 6.9). The fluorescence was measured at excitation and emission wavelengths of 485 and 530 nm, respectively, at 25°C for 60 min.

RESULTS

CPBF6 binds to α-amylase and γ-amylase. In order to identify cargo proteins that bind to CPBF6, we immunoprecipitated CPBF6 from the lysates of the transformant in which HA-tagged CPBF6 was ectopically expressed, by using an anti-HA antibody (Fig. 1A). SDS-PAGE analysis followed by silver staining revealed

TABLE 1 CPBF6-binding proteins identified by LC-MS/MS analysis

Excised band, mass (kDa)	AmoebaDB gene ID (GenBank accession no.)	Coverage (%)[a]	No. of detected peptides	Annotation	Predicted mass (kDa)
A, 100–150	EHI_178470 (XP_653036)	30.9	10	CPBF6	97.8
B, 75	EHI_044370 (XP_652381)	11.5	4	γ-Amylase	77.6
C, 50	EHI_023360 (XP_655636)	7.6	3	α-Amylase	56.7

[a] Coverage was determined based on the peptides with over 95% probability.

two major bands of 75 and 50 kDa (bands B and C) that were exclusively found in the immunoprecipitated sample from the CPBF6-HA strain, but not from CPBF8-HA or the HA control strain. These bands, together with a smeary region of about >120 kDa (band A), were excised and subjected to LC-MS/MS analysis (Table 1; see also Table S1 in the supplemental material). Bands B and C were identified as γ-amylase (XM_647289; EHI_044370) and α-amylase (XM_650544, EHI_023360), with 7.6% and 11.4% coverage, respectively. α-Amylase was previously demonstrated in phagosomes in our previous proteome analysis (31, 32). γ-Amylase was also confirmed to be present in phagosomes (see below). Band A was identified as CPBF6, and its apparent molecular mass based on SDS-PAGE (>120 kDa) was larger than the predicted size (99.3 kDa), suggesting that CPBF6 is posttranslationally modified, like CPBF8 (19). Western blotting with anti-α-amylase and anti-γ-amylase antibodies indicated that these amylases specifically bind to CPBF6 but not CPBF8 or HA (Fig. 1B).

CPBF6 is localized to phagosomes and lysosomes. As demonstrated above, CPBF6 bound to α- and γ-amylases, the former of which and CPBF6 were previously demonstrated in our phagosome proteome analysis (32). We examined localization of CPBF6 during phagocytosis of CHO cells. Trophozoites of the CPBF6-HA-expressing strain were incubated with CellTracker-loaded CHO cells for 60 min to allow ingestion of CHO cells. An immunofluorescence assay using anti-HA antibody showed that CPBF6 localized to phagosomes containing CHO cells (Fig. 2A). We estimated that approximately 81% of CHO-containing phagosomes had colocalized with CPBF6 ($n = 20$). As CPBF6 was also distributed to a large number of vesicles and vacuoles under quiescent (i.e., nonphagocytic) conditions, we next examined the nature of these compartments. CPBF6-HA associated with both small (360- to 720-nm diameter) and large (1.75- to 2.5-μm diameter) acidic organelles labeled with the membrane-diffusible LysoTracker dye under steady-state conditions (83% of LysoTracker positive vesicles/vacuoles were positive for CPBF6 [$n = 20$]) (Fig. 2B). The large CPBF6-associated vacuoles appeared to be multivesicular bodies (33) that contained vesicles, including LysoTracker-positive vesicles (Fig. 2B, arrowheads and inset). CPBF6 also nicely colocalized with pyridine nucleotide transhydrogenase (EhPNT) (27), which converts NADH to NADPH by direct transfer of a hydride ion via the proton gradient (Fig. 2C). Since antibodies against α- and γ-amylases were not usable in the immunofluorescence assay (data not shown), we attempted to examine localization of α- and γ-amylases by using *E. histolytica* lines that expressed carboxyl-terminal HA-tagged α- and γ-amylases. The fluorescent signal of HA-tagged α-amylase rarely overlapped that of PNT (Fig. 2D), which coincided with CPBF6 (Fig. 2C). This indicated that CPBF6 and α-amylase likely interact only transiently. Since HA-tagged γ-amylase wasn't detected in an *E. histolytica* transformant, as verified by immunoblot analysis, the localization of γ-amylase remains unknown.

Repression of *CPBF6* by gene silencing hampers trafficking of α-amylase and γ-amylase to phagosomes. To demonstrate the role of CPBF6, we created a *CPBF6* gene-silenced strain (CPBF6gs) with the genetic background of the G3 strain and in which amoebapore genes had already been repressed (21, 22). DNA microarray analysis verified that CPBF6 transcript was reduced by 2,419-fold while expression of other *CPBF* genes remained unchanged (Table 2).

We examined the protein amounts of α-amylase and γ-amylase in the whole-cell lysates and purified phagosomes from CPBF6gs and control strains by immunoblot analysis (Fig. 3A). The amounts of α-amylase in both the whole-cell lysate and, particularly, phagosomes from CPBF6gs were greatly reduced compared to the control strain. The protein amount of γ-amylase in phagosomes was also largely reduced, whereas γ-amylase in the whole-cell lysates could not be detected, due to either the scarcity of γ-amylase or the low sensitivity of the anti-γ-amylase antibody. Despite our efforts, including truncation at both the amino and carboxyl termini of CPBF6, we were unable to produce either full-length or truncated forms of CPBF6 in order to raise anti-CPBF6 antibody (data not shown). We also carried out the proteome analysis of isolated phagosomes from CPBF6gs and control strains. The percent coverage levels of the peptides corresponding to α-amylase and γ-amylase detected from phagosomes derived from the CPBF6gs strain were significantly lower than that detected from phagosomes of the control strain (Fig. 3B; see also Table S2 in the supplemental material). In contrast, the amount of CP5 (CP-A5), which was shown to be transported via CPBF1, in the whole-cell lysate and phagosomes remained unaffected; neither chaperonin 60 (Cpn60), the mitosomal control, nor cysteine synthase 3 (CS3), the cytoplasmic control, was detected in the phagosomes (Fig. 3A). Taken together, the repression of CPBF6 hampered, if not abolished, trafficking of α-amylase and γ-amylase to phagosomes. The amount of other proteins, namely, CP2 (EAL45256), hypothetical proteins EAL48580, EAL49001, and EAL46996, and the WD domain containing protein (EAL45537), detected in CPBF6gs strain, were also significantly lower than in control strain. Since these proteins were not detected in silver-stained SDS-PAGE gels of the CPBF-coimmunoprecipitated sample, repression of CPBF6 may have indirectly caused mistargeting of these proteins. We next measured amylase activities in the whole-cell lysates and the phagosome fractions from CPBF6gs and control strains (Fig. 3C). Unexpectedly, amylase activities toward the starch in both the whole-cell lysate and the isolated phagosomes were comparable between CPBF6gs and control strains.

We compared our newly created phagosome proteome from the G3 strain with our previous findings with the HM-1 strain (32). In the current study, we detected 345 proteins from phagosomes that were isolated after 60 min of coincubation of the trophozoites with beads (see Table S2). We compared phagosomal proteins detected in the present and previous studies at the same

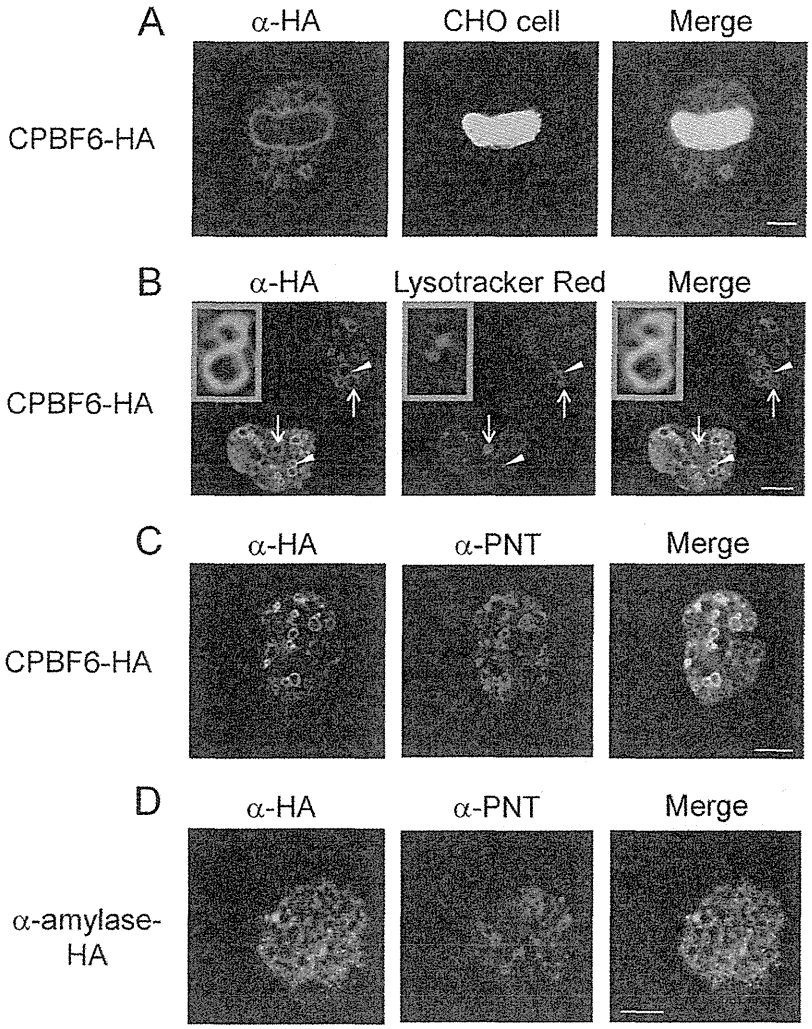

FIG 2 Localization of CPBF6 in *E. histolytica*. (A) Phagosome localization of CPBF6. Amoebae of the CPBF6-HA transformant were incubated with CellTracker Blue-stained CHO cells (blue) for 60 min, fixed, and reacted with anti-HA antibody and Alexa Fluor-488-conjugated anti-mouse IgG secondary antibody (green). Bar, 5 μm. (B) Lysosome localization of CPBF6. Amoebae of the CPBF6-HA transformant were labeled with LysoTracker Red (red) and subjected to an immunofluorescence assay with anti-HA antibody and Alexa Fluor-488-conjugated anti-mouse IgG secondary antibody (green). Bar, 10 μm. Arrows indicate representative large acidic vacuoles. Arrowheads indicate representative a small acidic vesicles of multivesicular bodies (MVB). The inset shows an enlarged image of the MVB. (C) Colocalization of CPBF6 and EhPNT. The cells of the CPBF6-HA transformant were fixed and reacted with anti-EhPNT antibody, Alexa Fluor-568-conjugated anti-rabbit IgG secondary antibody (red), anti-HA antibody, and Alexa Fluor-488-conjugated anti-mouse IgG secondary antibody (green). Bar, 10 μm. (D) Localization of α-amylase and EhPNT. The cells of the α-amylase-HA transformant were fixed and reacted with anti-EhPNT antibod and Alexa Fluor-568-conjugated anti-rabbit IgG secondary antibody (red) or anti-HA antibody and Alexa Fluor-488-conjugated anti-mouse IgG secondary antibody (green). Bar, 10 μm.

time point (60 min). Sixty-nine proteins were commonly detected in both studies, while 276 or 31 proteins were identified only in the present or previous study, respectively (at 60 min in reference 32) (see Tables S4 and S3 in the supplemental material). We categorized 67 common phagosomal proteins, based on protein functions (see Table S5). All data for phagosome proteomics can be found in Tables S2 to S5 of the supplemental material.

The serine-rich region of CPBF6 is important for cargo binding and phagosomal transport. CPBF6 contains, like CPBF8 (19) and CPBF7, an SRR located in the middle of the luminal portion of proteins. We previously demonstrated that the SRR of CPBF8 is involved in binding with the β-hexosaminidase α-subunit and lysozymes (19). We investigated whether the SRR of CPBF6 also plays a role in binding with its cargos. We created a transformant that expressed an HA-tagged mutant form of CPBF6 lacking the 43-aa-long SRR (CPBF6ΔSRR-HA). We immunoprecipitated CPBF6-HA and CPBF6ΔSRR-HA by using anti-HA antibody from lysates of the corresponding strains. The precipitated proteins were subjected to immunoblot analysis using anti-α-amylase and anti-γ-amylase antibodies (Fig. 4A). The amount of immunoprecipitated α-amylase and γ-amylase from the CPBF6ΔSRR-HA lysate was lower than that from the CPBF6-HA lysate. In addition, the immunofluorescence assay showed that CPBF6ΔSRR-HA was not localized to phagosomes (Fig. 4B). Only approximately 26% of phagosomes colocalized with CPBF6ΔSRR-HA, compared to

TABLE 2 Specific repression of *CPBF6* by gene silencing[a]

Gene	CPBF6gs strain	Control strain	Fold change
CPBF1	3,110 (±1,010)	2,780 (±268)	1.12
CPBF2	135 (±15.4)	141 (±16.7)	0.95
CPBF3	638 (±45.0)	482 (±18.4)	1.32
CPBF4	1,120 (±347)	1,040 (±269)	1.08
CPBF5	127 (±44.0)	136 (±38.9)	0.93
CPBF6	1.58 (±0.75)	3,820 (±87.8)	4.13×10^{-4}
CPBF7	1,730 (±282)	1,540 (±190)	1.13
CPBF8	5,620 (±556)	5,630 (±454)	1.00
CPBF9	311 (±24.9)	248 (±30.7)	1.26
CPBF10	123 (±90.2)	94.5 (±26.8)	1.30
CPBF11	96.3 (±14.6)	77.0 (±10.7)	1.25

[a] Total RNA was extracted from the CPBF6gs and control strains, and expression analysis was performed using a custom-made *E. histolytica* DNA microarray. Average (± standard deviation) normalized signal intensities from DNA microarrays were determined in triplicate and indicate relative levels of the transcripts, in arbitrary units, of *CPBF* genes (*CPBF1* to *CPBF11*) in the CPBF6gs and control strains. The fold change indicates the relative change in signal intensity in the CPBF6gs strain relative to that in the control strain.

>80% with full-length CPBF6-HA (n = 20). These data are consistent with the notion that the SRR in CPBF6 is important for both the binding to α-amylase and γ-amylase and for their phagosomal transport. Immunoblot analysis showed that CPBF6-HA was detected as a broad smeary band of 110 to 150 kDa (Fig. 1B and 4A), whereas CPBF6ΔSRR-HA was detected as an apparently single 100-kDa band. These data are consistent with the premise that the SRR contains posttranslational modifications.

The cytosolic domain is involved in the phagosomal trafficking of CPBF6. We speculated that the cytosolic domain containing the YxxΦ motif of CPBF proteins may also be involved in binding with accessory molecules and, therefore, plays an important role in the determination of localization. However, our previously study showed that the localization of CPBF1 was not altered by mutation of the YxxΦ motif, suggesting that the motif does not primarily determine its localization of CPBF1 (20). We asked if the cytoplasmic region containing the YxxΦ motif is involved in the phagosomal trafficking of CPBF6. We created two deletion mutants of CPBF6, CPBF6Δcytosol and CPBF6ΔNNGYHDLS, which lacked the entire 15-aa-long cytoso-

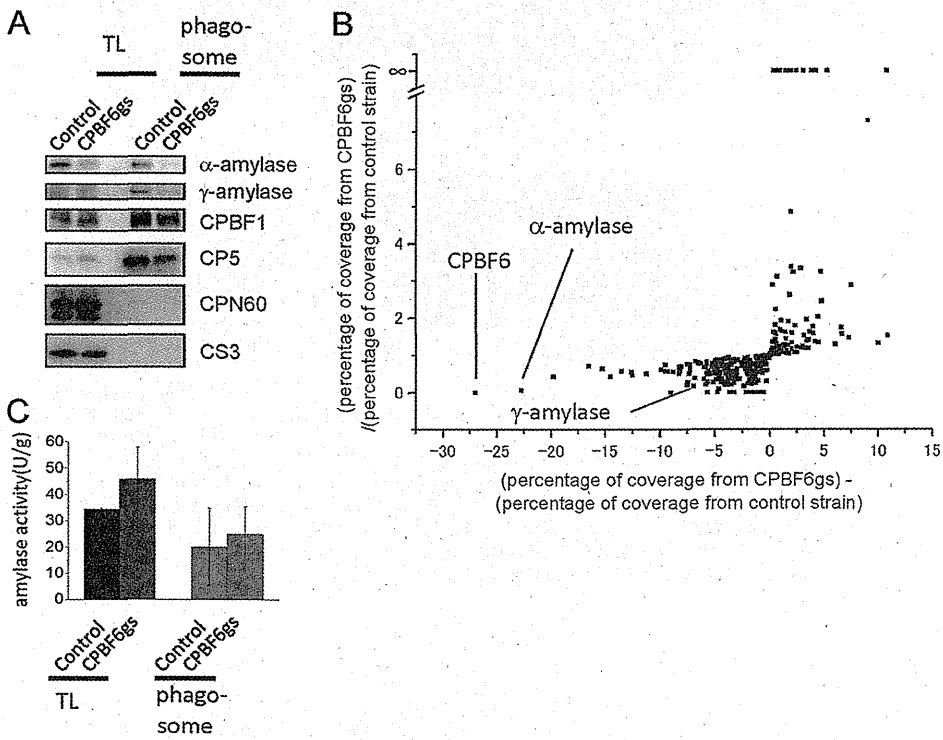

FIG 3 Phenotypic changes of *CPBF6* gene silencing. (A) Immunoblot analysis of the whole-cell lysate and the phagosome fraction. Approximately 20 μg of the whole-cell lysate and 2 μg of the phagosome fraction were electrophoresed by SDS-PAGE and subjected to immunoblot analysis using anti-α-amylase, anti-γ-amylase, CPBF1, CP5, Cpn60, and CS3 antibodies. CPBF1 and CP5 are phagosomal proteins, while CPN60 is a mitosomal marker and CS3 is a cytosolic marker. Faint smeary bands in the whole-cell lysate of the control and CPBF6gs strains, detected with anti-γ-amylase antibody, were considered background because of their low intensities compared to those in the phagosome fraction. (B) Proteomic analysis of isolated phagosomes from CPBF6gs and control strains. Each dot represents a protein identified from phagosomes. The x axis indicates the percentage of coverage from CPBF6gs minus the percentage of coverage from the control strain), and it is theoretically close to 0 when the repression of CPBF6 does not affect the trafficking of a protein. Similarly, y axis indicates the percentage of coverage from CPBF6gs divided by the percentage of coverage from the control strain, and it is close to 1 when the repression of CPBF6 does not affect the trafficking of a protein. Individual data are shown in Table S2 in the supplemental material. (C) Enzymatic activities of amylase in whole-cell lysates and phagosomes from CPBF6gs and control strains. The amoeba lysate, culture supernatant, or phagosomal fraction was mixed with 200 μg/ml of substrate solution containing BODIPY FL-conjugated DQ starch in 100 μl of 0.1 M MOPS (pH 6.9). The fluorescence was measured at excitation and emission wavelengths of 485 and 530 nm, respectively, at 25°C for 60 min. Data shown are the means ± standard deviations of three independent experiments.

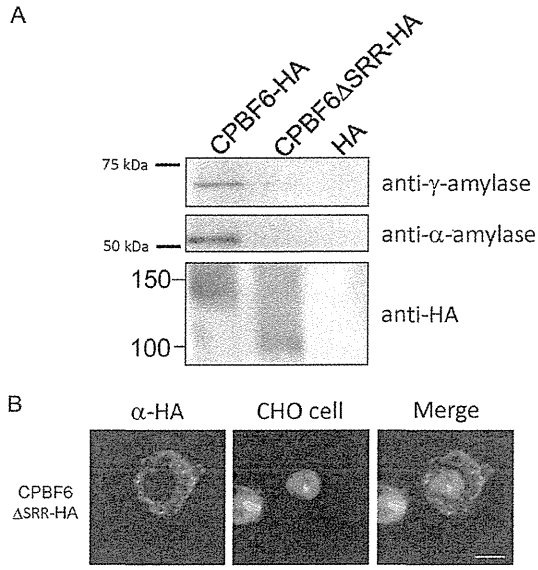

FIG 4 The SRR of CPBF6 is structurally important. (A) CPBF6-HA and CPBF6ΔSRR-HA were immunoprecipitated from corresponding expressing strains by using anti-HA-antibody-conjugated agarose, eluted with HA peptides, and subjected to SDS-PAGE and immunoblot analyses with anti-HA, anti-α-amylase, and anti-γ-amylase antibodies and appropriate secondary antibodies. (B) Localization of CPBF6ΔSRR-HA during phagocytosis. Amoebae were incubated with CellTracker Blue-stained CHO cells (blue) for 60 min, fixed, and reacted with anti-HA antibody and Alexa Fluor-488-conjugated anti-mouse IgG secondary antibody (green). Bar, 10 μm.

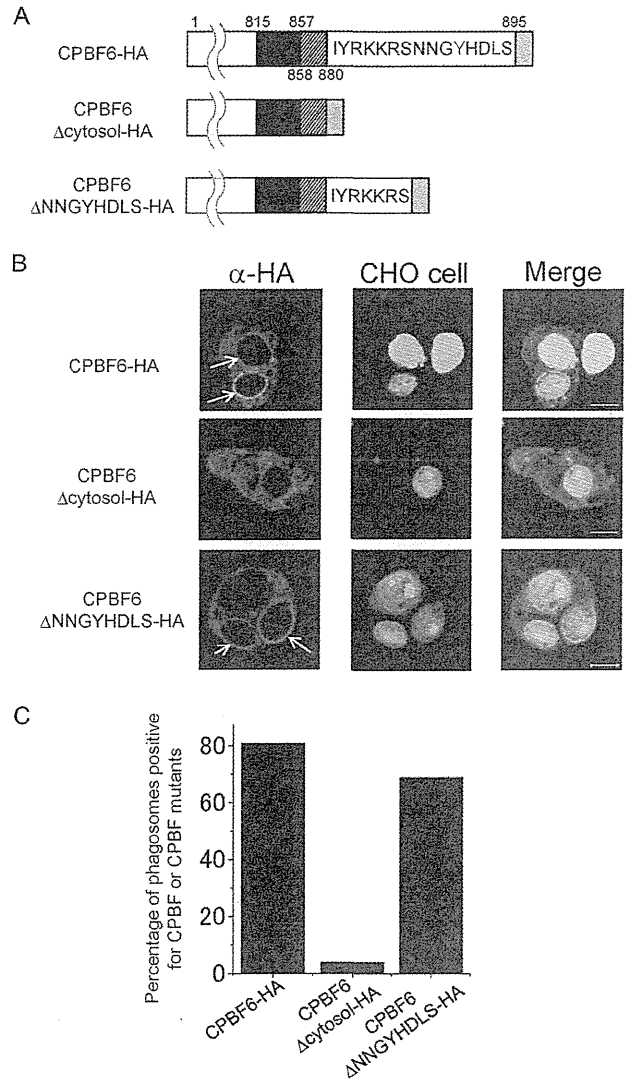

FIG 5 The carboxyl terminus of CPBF6 is required for the localization of CPBF6 to the phagosome. (A) Schematic representation of CPBF6-HA, CPBF6Δcytosol-HA, and CPBF6ΔNNGYHDLS-HA. Black boxes indicate the SRR. Gray boxes indicate the HA tag. Hatched boxes indicate the transmembrane region. Amino acid residues in the cytosolic region of the wild type and two CPBF6 mutants are shown, with tyrosine and leucine indicated in red. Amino acid positions are also depicted. (B) Localization of CPBF6-HA, CPBF6Δcytosol-HA, and CPBF6ΔNNGYHDLS-HA during phagocytosis. Amoebae were incubated with CellTracker Blue-stained CHO cells (blue) for 60 min, fixed, and reacted with anti-HA antibody and Alexa Fluor-488-conjugated anti-mouse IgG secondary antibody (green). Bar, 10 μm. Arrows indicate CPBF6-positive phagosomes. (C) Quantitative analysis of phagosomal localization of CPBF6-HA, CPBF6Δcytosol-HA, and CPBF6ΔNNGYHDLS-HA to phagosomes. The percentages of phagosomes with which wild-type or truncated CPBF6 colocalized in strains expressing CPBF6-HA, CPBF6Δcytosol-HA, or CPBF6ΔNNGYHDLS-HA are shown.

lic portion after the transmembrane domain or the 8-aa carboxyl-terminal portion containing the YxxΦ motif. We examined the localization of these proteins in an immunofluorescence assay (Fig. 5A and B). CPBF6Δcytosol showed localization dissimilar from that of CPBF6. Only 4% (n = 20) of phagosomes were positive with the anti-HA antibody in the CPBF6Δcytosol-HA transformant (Fig. 5C). In contrast, the percentage of phagosomes that localized with CPBF6ΔNNGYHDLS-HA was 69% (n = 20), comparable to that of wild-type CPBF6-HA (81%; n = 20). These results suggest that the cytosolic region, but not the YxxL motif itself, determines the phagosomal localization of CPBF6.

DISCUSSION

Cargo specificity of CPBF6. We demonstrated in the present study that one of the three most highly expressed CPBF proteins, CPBF6, selectively binds to putative α-amylase and γ-amylase and is essential for their trafficking to phagosomes. Together with our previous reports, we have now clearly shown that three major CPBFs, CPBF1 (20), -6 (this study), and -8 (19), have remarkable differences in their affinities toward cargo proteins: CPBF1 for CP-A1 and CP-A5, CPBF8 for β-hexosaminidase α-subunit and lysozymes, and CPBF6 for α-amylase and γ-amylase. The *E. histolytica* genome apparently encodes six proteins annotated as α-amylase. Among them, only one α-amylase (EHI_023360) was identified in this study, by virtue of its ability to bind to CPBF6. Furthermore, phagosome proteome analysis showed that two α-amylases (EHI_023360 and EHI_152880) are transported to phagosomes in the wild-type amoeba, but *CPBF6* gene silencing did not affect the transport of these amylases (EHI_023360 and EHI_152880) to phagosomes, although it abolished transport of another α-amylase (EHI_023360). Therefore, α-amylase (EHI_023360) appears to be a major, and perhaps the sole, α-amylase transported via CPBF6. In contrast, γ-amylase is encoded by a single gene in the *E. histolytica* genome. These findings altogether underline the strict cargo specificity of CPBF6 in trafficking of lysosomal enzymes. As we

did not directly sequence the eluate of immunoprecipitation, the whole spectrum of cargos that CPBF6 binds, including ones identified in this study, remains unknown.

Differences in structural determinants for cargo binding of CPBF6. CPBF8 has an SRR, which is essential for binding to both β-hexosaminidase α-subunit and lysozymes (19). In this study, we found that the SRR is apparently conserved in CPBF6 and is structurally important. In contrast, CPBF1 apparently lacks the SRR, suggesting that the SRR is not required for binding of CPBF1 to CPs (20). Recently, we found that another member of the family, CPBF10, binds to two isotypes of α-amylase (EHI_023360 and EHI_153100) (K. Marumo et al., unpublished data). Since CPBF10 apparently lacks the SRR and yet binds to α-amylase (EHI_023360), CPBF6 may also bind to α-amylase (EHI_023360) via a portion other than the SRR. Phylogenetic analysis of CPBFs suggests that CPBF6 belongs to the same clade as CPBF7, -8, and -10 (20). This may partially explain the overlapping cargo specificity of CPBF6 and CPBF10. These data also imply that an ancestor of CPBF6, -7, -8, and -10 may have recognized ancestral α-amylase, which is closest to the extant EHI_023360, and CPBF6 and -10 have further evolved to gain additional binding abilities while CPBF8 has lost its binding capacity to α-amylase and gained the binding capacity for the β-hexosaminidase α-subunit and lysozymes.

Physiological functions of CPBF6 and its cargos. We have unequivocally demonstrated the cargo specificity of CPBF6. As shown by Western blotting and proteome analysis, phagosome transport of α-amylase and γ-amylase was severely affected by *CPBF6* gene silencing. The amount of α-amylase and γ-amylase in the whole-cell lysate from CPBF6gs also decreased compared to the control strain. This observation was similar to that for CPBF8gs, where the amounts of β-hexosaminidase α-subunit and lysozymes in the whole-cell lysates were greatly reduced (19). Although deletion or repression of hydrolase receptors often causes missecretion of cargos (20), gene silencing of *CPBF8* did not result in missecretion of the β-hexosaminidase α-subunit and lysozymes. This can be explained by swift degradation of non- or mistargeted α-amylase and γ-amylase by proteasomes in the CPBF8gs strain. Although we have clearly demonstrated that phagosomal transport of α-amylase and γ-amylase is mediated by CPBF6, enzymatic activities toward the starch were comparable between the control strain and CPBF6gs. These data indicate that another protein(s), e.g., β-amylase, compensates for the phagosomal amylase activities in the CPBF6gs strain. However, an increase of β-amylase in phagosomes from the CPBF6gs strain, compared to that from the control strain, which was detected by proteomic analysis (see Table S2 in the supplemental material), did not prove to be statistically significant. Alternatively, the current assay method used in this study did not allow measurement of the specific activities of the putative amylases transported via CPBF6. As the percent coverage of β-amylase (EAL48510) was higher in the CPBF6gs strain than in the control strain, the increased β-amylase may have compensated for the overall amylase activity in the phagosome fraction from the CPBF6gs strain. Although the amylase activity was also measured at low pH, which is favorable for γ-amylase, it was comparable between the CPBF6gs and control strains (data not shown).

α-Amylase (EHI_023360) contains the maltase (3.31 e−5) and α-phosphotrehalase (4.81 e−4) domains, based on a pfam search. γ-Amylase (EHI_044370) has similarity with glucoamylase from *Thermoactiomyces vulgaris* (2 e−9), which has been shown to have high hydrolytic activity toward maltooligosaccharides (34). The substrates of α-amylase and γ-amylase should be determined in the future to allow a better understanding of the biological and physiological roles of CPBF6.

Mechanisms for phagosomal localization of CPBF6. Our mutation study showed that the YxxL motif does not determine the phagosomal localization of CPBF6. Our previous study with CPBF1 also suggested that this motif is not required for localization of CPBF1 to the endoplasmic reticulum (ER) and phagosomes (20). Thus, we concluded that the YxxL motif is not likely involved in the recruitment of this family of receptors/carriers in *E. histolytica*. This is surprising, as the major components of the AP complex and clathrins are conserved in *E. histolytica* (35, 36), and the motif is known to bind to the μ-subunit of the complex.

We further demonstrated that deletion of the cytosolic region containing a stretch of positively charged amino acids, IYRKKRS, close to the transmembrane region abolished phagosomal localization of CPBF6. In *Saccharomyces cerevisiae*, it has been reported that lysines and arginines in the carboxyl-terminal region are involved in the interaction with phospholipids (37) and that the higher the number of lysine/arginine residues in the region, the higher is the affinity of the protein with phospholipids. It was also demonstrated that negatively charged phosphatidylinositides such as PI3P and PIP3, accumulate in phagosomes (13–15). Thus, it is plausible that lysines and arginines in the cytosolic region of CPBF6 are involved in the recognition of a phospholipid(s) on phagosomal membranes that determines the recruitment of CPBF6 to phagosomes. CPBF1, -7, and -8 were previously found in phagosomes and have a lysine-/arginine-rich region downstream of the transmembrane region, similar to CPBF6 (19). Altogether, we tentatively propose that the lysine-/arginine-rich cytosolic region is responsible for the recruitment of these CPBF members to phagosomes.

Differential localization of CPBF1, -6, and -8 and colocalization of CPBF6 with PNT. CPBF6 is distributed to the membrane of lysosomes and multivesicular bodies in the quiescent state and translocated to phagosomes during phagocytosis. The localization and dynamism of CPBF6 were similar to those of CPBF8 (19). In contrast, CPBF1 showed different localization from CPBF6 and CPBF8; CPBF1 mainly localizes to the ER and occasionally to phagosomes, but seldom to lysosomes (20). Phylogenetic analysis of CPBFs from three species of *Entamoeba* (also discussed above) clearly indicated that CPBF6, -7, 08 to -8, and -10 form monophyly (20), suggesting evolutionary kinship among them. CPBF1 appears to have diverged from the clade consisting of CPBF3, 04 to -4, and -11 and CPBF6, -7, -8, and -10 at the earlier stage of evolution. Such an evolutionary distance between CPBF6 and -8 and CPBF1 may result in the different localization of CPBF6 and -8 and CPBF1. The colocalization of both CPBF6 (Fig. 2C) and CPBF8 (19) with EhPNT was striking. PNT is distributed to both LysoTracker-stainable acidic (late endosomes, lysosomes, and phagosomes) and nonacidic vesicles and vacuoles (27), and therefore is not necessarily a lysosomal marker, despite the fact that PNT utilizes the proton gradient across the membrane. Thus, it is tempting to speculate that CPBF6/8 and PNT are cotransported and that the enzymatic reactions of putative α-amylase, γ-amylase, β-hexosaminidase α-subunit, and lysozymes transported by CPBF6/8, require NADPH produced by PNT. The mechanisms of localization of PNT to lysosomes, endosomes, and phagosomes

are still unknown. We previously demonstrated that all domains, such as the amino-terminal extension, 11–13 transmembrane, and linker regions are essential for the vesicular/vacuolar distribution of PNT (27). However, in contrast to CPBF6, no apparent lysine-/arginine-rich region is present in PNT.

ACKNOWLEDGMENTS

We are grateful to Nicholas Sherman, W.M. Keck Biomedical Mass Spectrometry Laboratory at the University of Virginia, for technical support on MS analyses. We are also grateful to Kazuo Ebine and Kisaburo Nagamune for helpful discussions.

This work was supported by a Grant-in-Aid for Scientific Research from the Ministry of Education, Culture, Sports, Science and Technology (MEXT) of Japan (23117001, 23117005, and 23390099), a Grant-in-Aid on Bilateral Programs of Joint Research Projects and Seminars from the Japan Society for the Promotion of Science, a Grant-in-Aid on Strategic International Research Cooperative Program (SICP) from the Japan Science and Technology Agency, a grant for research on emerging and re-emerging infectious diseases from the Ministry of Health, Labor and Welfare (MHLW) of Japan (H23-Shinkosaiko-ippan-014), a grant for research to promote the development of anti-AIDS pharmaceuticals from the Japan Health Sciences Foundation (KHA1101), and by the Global COE Program (Global COE for Human Metabolomic Systems Biology) from MEXT, Japan.

REFERENCES

1. **Bracha R, Kobiler D, Mirelman D.** 1982. Attachment and ingestion of bacteria by trophozoites of *Entamoeba histolytica*. Infect. Immun. 36:396–406.
2. **Tsutsumi V, Ramírez-Rosales A, Lanz-Mendoza H, Shibayama M, Chávez B, Rangel-López E, Martínez-Palomo A.** 1992. *Entamoeba histolytica*: erythrophagocytosis, collagenolysis, and liver abscess production as virulence markers. Trans. R. Soc. Trop. Med. Hyg. 86:170–172.
3. **Guerrant RL, Brush J, Ravdin JI, Sullivan JA, Mandell GL.** 1981. Interaction between *Entamoeba histolytica* and human polymorphonuclear neutrophils. J. Infect. Dis. 143:83–93.
4. **Bracha R, Mirelman D.** 1984. Virulence of *Entamoeba histolytica* trophozoites. Effects of bacteria, microaerobic conditions, and metronidazole. J. Exp. Med. 160:353–368.
5. **Hirata KK, Que X, Melendez-Lopez SG, Debnath A, Myers S, Herdman DS, Orozco E, Bhattacharya A, McKerrow JH, Reed SL.** 2007. A phagocytosis mutant of *Entamoeba histolytica* is less virulent due to deficient proteinase expression and release. Exp. Parasitol. 115:192–199.
6. **Katz U, Ankri S, Stolarsky T, Nuchamowitz Y, Mirelman D.** 2002. *Entamoeba histolytica* expressing a dominant negative N-truncated light subunit of its Gal-lectin are less virulent. Mol. Biol. Cell 13:4256–4265.
7. **Orozco E, Guarneros G, Martinez-Palomo A, Sánchez T.** 1983. *Entamoeba histolytica*. Phagocytosis as a virulence factor. J. Exp. Med. 158: 1511–1521.
8. **Que X, Brinen LS, Perkins P, Herdman S, Hirata K, Torian BE, Rubin H, McKerrow JH, Reed SL.** 2002. Cysteine proteinases from distinct cellular compartments are recruited to phagocytic vesicles by *Entamoeba histolytica*. Mol. Biochem. Parasitol. 119:23–32.
9. **Andrä J, Herbst R, Leippe M.** 2003. Amoebapores, archaic effector peptides of protozoan origin, are discharged into phagosomes and kill bacteria by permeabilizing their membranes. Dev. Comp. Immunol. 27: 291–304.
10. **Mann BJ.** 2002. Structure and function of the *Entamoeba histolytica* Gal/GalNAc lectin. Int. Rev. Cytol. 216:59–80.
11. **Petri WA, Jr, Haque R, Mann BJ.** 2002. The bittersweet interface of parasite and host: lectin-carbohydrate interactions during human invasion by the parasite *Entamoeba histolytica*. Annu. Rev. Microbiol. 56:39–64.
12. **Voigt H, Olivo JC, Sansonetti P, Guillén N.** 1999. Myosin IB from *Entamoeba histolytica* is involved in phagocytosis of human erythrocytes. J. Cell Sci. 112:1191–1201.
13. **Byekova YA, Powell RR, Welter BH, Temesvari LA.** 2010. Localization of phosphatidylinositol (3,4,5)-trisphosphate to phagosomes in *Entamoeba histolytica* achieved using glutathione S-transferase- and green fluorescent protein-tagged lipid biosensors. Infect. Immun. 78:125–137.
14. **Ghosh SK, Samuelson J.** 1997. Involvement of p21racA, phosphoinositide 3-kinase, and vacuolar ATPase in phagocytosis of bacteria and erythrocytes by *Entamoeba histolytica*: suggestive evidence for coincidental evolution of amebic invasiveness. Infect. Immun. 65:4243–4249.
15. **Nakada-Tsukui K, Okada H, Mitra BN, Nozaki T.** 2009. Phosphatidylinositol-phosphates mediate cytoskeletal reorganization during phagocytosis via a unique modular protein consisting of RhoGEF/DH and FYVE domains in the parasitic protozoon *Entamoeba histolytica*. Cell. Microbiol. 11:1471–1491.
16. **Somlata Bhattacharya S, Bhattacharya A.** 2011. A C2 domain protein kinase initiates phagocytosis in the protozoan parasite *Entamoeba histolytica*. Nat. Commun. 2:230.
17. **Boettner DR, Huston CD, Linford AS, Buss SN, Houpt E, Sherman NE, Petri WA, Jr.** 2008. *Entamoeba histolytica* phagocytosis of human erythrocytes involves PATMK, a member of the transmembrane kinase family. PLoS Pathog. 4:e8. doi:10.1371/journal.ppat.0040008.
18. **Labruyère E, Zimmer C, Galy V, Olivo-Marin Guillén J-CN.** 2003. EhPAK, a member of the p21-activated kinase family, is involved in the control of *Entamoeba histolytica* migration and phagocytosis. J. Cell Sci. 116:61–71.
19. **Furukawa A, Nakada-Tsukui K, Nozaki T.** 2012. Novel transmembrane receptor involved in phagosome transport of lysozymes and β-hexosaminidase in the enteric protozoan *Entamoeba histolytica*. PLoS Pathog. 8:e1002539. doi:10.1371/journal.ppat.1002539.
20. **Nakada-Tsukui K, Tsuboi Furukawa K, Yamada A, Nozaki Y, T.** 2012. A novel class of cysteine protease receptors that mediate lysosomal transport. Cell. Microbiol. 14:1299–1317.
21. **Bracha R, Nuchamowitz Y, Mirelman D.** 2003. Transcriptional silencing of an amoebapore gene in *Entamoeba histolytica*: molecular analysis and effect on pathogenicity. Eukaryot. Cell 2:295–305.
22. **Zhang H, Alramini H, Tran V, Singh U.** 2011. Nucleus-localized antisense small RNAs with 5′-polyphosphate termini regulate long term transcriptional gene silencing in *Entamoeba histolytica* G3 strain. J. Biol. Chem. 286:44467–44479.
23. **Diamond LS, Mattern CF, Bartgis IL.** 1972. Viruses of *Entamoeba histolytica*. I. Identification of transmissible virus-like agents. J. Virol. 9:326–341.
24. **Diamond LS, Harlow DR, Cunnick CC.** 1978. A new medium for the axenic cultivation of *Entamoeba histolytica* and other Entamoeba. Trans. R. Soc. Trop. Med. Hyg. 72:431–432.
25. **Saito-Nakano Y, Mitra BN, Nakada-Tsukui K, Sato D, Nozaki T.** 2007. Two Rab7 isotypes, EhRab7A and EhRab7B, play distinct roles in biogenesis of lysosomes and phagosomes in the enteric protozoan parasite *Entamoeba histolytica*. Cell. Microbiol. 9:1796–1808.
26. **Nozaki T, Asai T, Sanchez LB, Kobayashi S, Nakazawa M, Takeuchi T.** 1999. Characterization of the gene encoding serine acetyltransferase, a regulated enzyme of cysteine biosynthesis from the protist parasites *Entamoeba histolytica* and Entamoeba dispar. Regulation and possible function of the cysteine biosynthetic pathway in Entamoeba. J. Biol. Chem. 274:32445–32452.
27. **Yousuf MA, Mi-Ichi F, Nakada-Tsukui K, Nozaki T.** 2010. Localization and Targeting of an unusual pyridine nucleotide transhydrogenase in *Entamoeba histolytica*. Eukaryot. Cell 9:926–933.
28. **Gilchrist CA, Houpt E, Trapaidze N, Fei Z, Crasta O, Asgharpour A, Evans C, Martino-Catt S, Baba DJ, Stroup S, Hamano S, Ehrenkaufer G, Okada M, Singh U, Nozaki T, Mann BJ, Petri WA, Jr.** 2006. Impact of intestinal colonization and invasion on the *Entamoeba histolytica* transcriptome. Mol. Biochem. Parasitol. 147:163–176.
29. **Husain A, Jeelani G, Sato D, Nozaki T.** 2011. Global analysis of gene expression in response to L-cysteine deprivation in the anaerobic protozoan parasite *Entamoeba histolytica*. BMC Genomics 12:275. doi:10.1186/1471-2164-12-275.
30. **Penuliar GM, Furukawa A, Nakada-Tsukui K, Husain A, Sato D, Nozaki T.** 2012. Transcriptional and functional analysis of trifluoromethionine resistance in *Entamoeba histolytica*. J. Antimicrob. Chemother. 67:375–386.
31. **Okada M, Huston CD, Mann BJ, Petri WA, Kita K, Nozaki T.** 2005. Proteomic analysis of phagocytosis in the enteric protozoan parasite *Entamoeba histolytica*. Eukaryot. Cell 4:827–831.
32. **Okada M, Huston CD, Oue M, Mann BJ, Petri WA, Jr, Kita K, Nozaki T.** 2006. Kinetics and strain variation of phagosome proteins of *Entamoeba histolytica* by proteomic analysis. Mol. Biochem. Parasitol. 145: 171–183.

33. Saito-Nakano Y, Yasuda T, Nakada-Tsukui K, Leippe M, Nozaki T. 2004. Rab5-associated vacuoles play a unique role in phagocytosis of the enteric protozoan parasite *Entamoeba histolytica*. J. Biol. Chem. 279: 49497–49507.
34. Uotsu-Tomita R, Tonozuka T, Sakai H, Sakano Y. 2001. Novel glucoamylase-type enzymes from *Thermoactinomyces vulgaris* and *Methanococcus jannaschii* whose genes are found in the flanking region of the a-amylase genes. Appl. Microbiol. Biotechnol. 56:465–473.
35. Clark CG, Alsmark UCM, Tazreiter M, Saito-Nakano Y, Ali V, Marion S, Weber C, Mukherjee C, Bruchhaus I, Tannich E, Leippe M, Sicheritz-Ponten T, Foster PG, Samuelson J, Noël CJ, Hirt RP, Embley TM, Gilchrist CA, Mann BJ, Singh U, Ackers JP, Bhattacharya S, Bhattacharya A, Lohia A, Guillén N, Duchêne M, Nozaki T, Hall N. 2007. Structure and content of the *Entamoeba histolytica* genome. Adv. Parasitol. 65:51–190.
36. Loftus B, Anderson I, Davies R, Alsmark UCM, Samuelson J, Amedeo P, Roncaglia P, Berriman M, Hirt RP, Mann BJ, Nozaki T, Suh B, Pop M, Duchene M, Ackers J, Tannich E, Leippe M, Hofer M, Bruchhaus I, Willhoeft U, Bhattacharya A, Chillingworth T, Churcher C, Hance Z, Harris B, Harris D, Jagels K, Moule S, Mungall K, Ormond D, Squares R, Whitehead S, Quail MA, Rabbinowitsch E, Norbertczak H, Price C, Wang Z, Guillén N, Gilchrist C, Stroup SE, Bhattacharya S, Lohia A, Foster PG, Sicheritz-Ponten T, Weber C, Singh U, Mukherjee C, El-Sayed NMWAP, Jr, Clark CG, Embley TM, Barrell B, Fraser CM, Hall N. 2005. The genome of the protist parasite *Entamoeba histolytica*. Nature 433:865–868.
37. Scheglmann D, Werner K, Eiselt G, Klinger R. 2002. Role of paired basic residues of protein C-termini in phospholipid binding. Protein Eng. 15: 521–527.

OPEN ACCESS Freely available online PLoS PATHOGENS

Novel Transmembrane Receptor Involved in Phagosome Transport of Lysozymes and β-Hexosaminidase in the Enteric Protozoan *Entamoeba histolytica*

Atsushi Furukawa[1,2], Kumiko Nakada-Tsukui[1], Tomoyoshi Nozaki[1,3]*

1 Department of Parasitology, National Institute of Infectious Diseases, Toyama, Shinjuku-ku, Tokyo, Japan, **2** Department of Parasitology, Gunma University Graduate School of Medicine, Showa-machi, Maebashi, Japan, **3** Graduate School of Life and Environmental Sciences, University of Tsukuba, Tennoudai, Tsukuba, Ibaraki, Japan

Abstract

Lysozymes and hexosaminidases are ubiquitous hydrolases in bacteria and eukaryotes. In phagocytic lower eukaryotes and professional phagocytes from higher eukaryotes, they are involved in the degradation of ingested bacteria in phagosomes. In *Entamoeba histolytica*, which is the intestinal protozoan parasite that causes amoebiasis, phagocytosis plays a pivotal role in the nutrient acquisition and the evasion from the host defense systems. While the content of phagosomes and biochemical and physiological roles of the major phagosomal proteins have been established in *E. histolytica*, the mechanisms of trafficking of these phagosomal proteins, in general, remain largely unknown. In this study, we identified and characterized for the first time the putative receptor/carrier involved in the transport of the above-mentioned hydrolases to phagosomes. We have shown that the receptor, designated as cysteine protease binding protein family 8 (CPBF8), is localized in lysosomes and mediates transport of lysozymes and β-hexosaminidase α-subunit to phagosomes when the amoeba ingests mammalian cells or Gram-positive bacillus *Clostridium perfringens*. We have also shown that the binding of CPBF8 to the cargos is mediated by the serine-rich domain, more specifically three serine residues of the domain, which likely contains trifluoroacetic acid-sensitive O-phosphodiester-linked glycan modifications, of CPBF8. We further showed that the repression of CPBF8 by gene silencing reduced the lysozyme and β-hexosaminidase activity in phagosomes and delayed the degradation of *C. perfringens*. Repression of CPBF8 also resulted in decrease in the cytopathy against the mammalian cells, suggesting that CPBF8 may also be involved in, besides the degradation of ingested bacteria, the pathogenesis against the mammalian hosts. This work represents the first case of the identification of a transport receptor of hydrolytic enzymes responsible for the degradation of microorganisms in phagosomes.

Citation: Furukawa A, Nakada-Tsukui K, Nozaki T (2012) Novel Transmembrane Receptor Involved in Phagosome Transport of Lysozymes and β-Hexosaminidase in the Enteric Protozoan *Entamoeba histolytica*. PLoS Pathog 8(2): e1002539. doi:10.1371/journal.ppat.1002539

Editor: Patricia J. Johnson, University of California Los Angeles, United States of America

Received August 15, 2011; **Accepted** January 5, 2012; **Published** February 23, 2012

Funding: This work was supported by a Grant-in-Aid for Scientific Research from the Ministry of Education, Culture, Sports, Science and Technology (MEXT) of Japan (18GS0314, 18050006, 18073001, 20390119, 23390099) and to K.N-T. (18790291, 20790323), a grant for research on emerging and re-emerging infectious diseases from the Ministry of Health, Labour and Welfare of Japan (H20-Shinko-ippan-016, H23-Shinko-ippan-014), a grant for research to promote the development of anti-AIDS pharmaceuticals from the Japan Health Sciences Foundation (KAA1551, KHA1101), and by Global COE Program (Global COE for Human Metabolomic Systems Biology) from MEXT, Japan. The funders had no role in study design, data collection and analysis, decision to publish, or preparation of the manuscript.

Competing Interests: The authors have declared that no competing interests exist.

* E-mail: nozaki@nih.go.jp

Introduction

Lysozymes (EC 3.2.1.17) are the antibacterial protein that has an ability to damage the cell wall of bacteria [1]. The enzyme acts by catalyzing the hydrolysis of 1,4-beta-linkages between *N*-acetylmuramic acid and *N*-acetyl-D-glucosamine in peptidoglycans and between the *N*-acetyl-D-glucosamine residues in chitodextrins. While biochemical [2], functional [3], and structural [4] features of lysozymes have been well established, the mechanisms for intracellular trafficking and secretion remain poorly characterized except for the report that showed that condroitin sulfate is involved in lysosomal targeting of lysozymes [5]. Hexosaminidase (EC 3.2.1.52) is involved in the hydrolysis of terminal N-acetyl-D-hexosamine residues in hexosaminides. Three dimeric isozymes of β-hexosaminidase are formed by the combination of α and β subunits, encoded by *HEXA* and *HEXB* genes, respectively. β-Hexosaminidase and the cofactor GM2 activator protein catalyze the degradation of the GM2 gangliosides containing terminal N-acetyl hexosamines [6]. Mutations in *HEXA* gene decrease the hydrolysis of GM2 gangliosides, which is the main cause of Tay-Sachs disease, whereas mutations in *HEXB* gene results in Sandhoff disease [7]. The trafficking mechanism of β-hexosaminidase via mannose-6-phosphate receptor has been well studied in mouse lymphoma and myeloma cell [8–10]. However, the mechanisms of trafficking of β-hexosaminidase in eukaryotes besides mammals remain to be discovered.

Lysozyme and β-hexosaminidase are abundant components found in phagosomes from *Entamoeba histolytica* [11,12], which is the anaerobic or microaerophilic protozoan parasite, causing amebic dysentery and amebic liver abscesses in an estimated 10 million cases annually [13]. However, the role and intracellular trafficking of these enzymes remain unknown. Phagocytosis and phagosome biogenesis seems to play a pivotal role in pathogenesis in *E. histolytica* [14]. *E. histolytica* is capable of internalizing

Author Summary

Phagocytosis is the cellular process of engulfing solid particles to form an internal phagosome in protozoa, algae, and professional phagocytes of multicellular eukaryotic organisms. In phagocytic protozoa, phagocytosis is involved in the acquisition of nutrients, and the evasion from the host immune system and inflammation. While hydrolytic enzymes that are essential for the efficient and regulated degradation of phagocytosed particles, such as bacteria, fungi, and eukaryotic organisms, have been characterized, the mechanisms of the transport of these proteins are poorly understood. In the present study, we have demonstrated, for the first time, the molecular mechanisms of how the digestive enzymes are transported to phagosomes. Understanding of such mechanisms of the transport of phagosomal proteins at the molecular level may lead to the identification of a novel target for the development of new preventive measures against parasitic infections caused by phagocytic protozoa.

extracellular particles by phagocytosis. The amebic trophozoites ingest microorganisms in the large intestine [15,16], and host cells including non-immune cells [17], and immune cells [18] during tissue invasion. It has been well-established that in vitro and in vivo virulence correlates well with the ability of phagocytosis [14,19,20]. Furthermore, phagosomes contain a panel of proteins that were shown to be crucial in pathogenesis such as cysteine proteases (CPs) [21], amoeba pores [22], and galactose/N-acetylgalactosamine-specific lectin [23,24], proteins involved in cytoskeletal reorganization [25,26], vesicular trafficking [27–29], and signal transduction [30,31]. Therefore, understanding the molecular mechanisms of phagocytosis and phagosome biogenesis as well as the role and trafficking of individual phagosomal proteins in phagosomes, should help to understand underlying links between phagocytosis and pathogenicity.

Recently, the proteins and mechanisms involved in phagocytosis have been demonstrated. For instance, the surface Ca^{2+}-binding kinase (C2PK) has shown to be involved in the initiation of phagocytosis [31]. The antisense inhibition of C2PK caused inhibition of the initiation of erythrophagocytosis. It has also been shown that surface transmembrane kinase (TMK96) and p21-activated kinase (PAK) play an important role in phagocytosis of human erythrocytes [32,33]. The unconventional myosin, myosin IB, was shown to be involved in cytoskeleton rearrangement during phagocytosis [25,26]. Furthermore, phosphatidylinositides also play critical roles during phagocytosis [34,35]. Our previous proteomic studies, where 159 proteins were identified from purified phagosomes [11,12], also suggested a direct link between phagosome biogenesis and pathogenesis, as phagosomes contained a panel of proteins that were shown to be crucial in pathogenesis described above. Furthermore, the proteins that are implicated for degradation of phagocytosed bacteria, e.g. amoebapores [22], lysozymes, and β-hexosaminidase, as well as other hydrolytic enzymes such as amylase and ribonuclease were also demonstrated in phagosomes. While both the constituents of phagosomes and the kinetics of their recruitment are known, very little is known on how these proteins are transported to phagosomes. Recently, we discovered a putative transmembrane receptor for cysteine proteases from *E. histolytica*, which preferentially binds to CP5 (Nakada-Tsukui K, et al., unpublished data), which is directly implicated in the pathogenesis [36–38]. The *E. histolytica* genome contained a total of 11 members showing significant mutual identity and structural conservation to the transmembrane cysteine protease receptor: the signal peptide at the amino terminus, a single transmembrane domain close to the carboxyl terminus, and the YxxΦ motif at the carboxyl terminus. This family of proteins was designated as cysteine protease binding family proteins 1–11 (CPBF1-11). In the present study, we characterized one of the most highly expressed CPBF genes among the family, *CPBF8*. We showed that CPBF8 localizes to phagosomes during phagocytosis, while it is distributed to the acidic compartment in steady state. Affinity immunoprecipitation followed by LC-MS/MS analysis showed that CPBF8 specifically bound to lysozymes and β-hexosaminidase α-subunit. Repression of CPBF8 by gene silencing reduced lysozyme and β-hexosaminidase activities in phagosomes, and caused a defect of digestion of ingested bacteria.

Results

Localization of CPBF8

We examined the localization of CPBF8 during phagocytosis of CHO cells. Trophozoites of CPBF8-HA-expressing strain were incubated with CellTracker-loaded CHO cells for 10 to 60 min to allow ingestion of CHO cells. Immunofluorescence assay using anti-HA antibody showed that CPBF8 was localized to phagosomes containing CHO cells at all time points (10, 30, and 60 mins) (Figure 1A). CPBF8 remained associated with phagosomes in the course of phagocytosis: the percentage of colocalization did not significantly changed (84, 92 and 82% at 10, 30, and 60 min, respectively). Immunofluorescence image of the amoeba undergoing engulfment revealed that CPBF8 localized to the basolateral portion of a phagosome, and excluded from the tunnel-like structure connecting a phagosome and the CHO cell being aspirated [35].

As immunofluorescence assay showed that CPBF8 was also distributed to a large number of vesicles and vacuoles under quiescent (i.e., non-phagocytic) conditions, we examined the nature of these compartments. CPBF8-HA was associated with the acidic organelles labeled with membrane-diffusible LysoTracker under steady-state conditions (60% of LysoTracker-positive vesicles/vacuoles was positive for CPBF8) (Figure 1B). CPBF8 colocalized nicely with a vacuolar membrane protein, pyridine nucleotide transhydrogenase, *Eh*PNT, which converts NADPH and NADH using the proton gradient across the membrane [39] (Figure 1C). It has been shown that *Eh*PNT is localized to the acidic compartment in steady state and transported to phagosomes upon phagocytosis [40].

CPBF8 binds to β-hexosaminidase α-subunit and lysozymes

To identify potential cargo proteins that CPBF8 binds and carries to phagosomes, we immunoprecipitated proteins that bind to CPBF8, from the lysates of the transformant where HA-tagged CPBF8 was ectopically expressed (Figure 2). Silver stained SDS-PAGE gel revealed three major bands of about >120, 60, and 20 kDa (bands C, E, and F) and three minor bands of about >300, >200, and 75 kDa (bands A, B, and D) exclusively found in the immunoprecipitated sample from CPBF8-HA strain, but not from HA control strain. These bands were excised and subjected to LC-MS/MS analysis (Table 1 and Table S1). Smeary band C, which showed an apparent molecular mass of ~130 kDa on SDS-PAGE was identified as CPBF8 itself; the apparent size was larger than the predicted size (99.3 kDa), suggestive of post-translational modifications or aberrant structure (see below). Band E was identified as β-hexosaminidase α-subunit (XP_657529; EHI_148130) with 19.7% coverage. Band F was identified as a mixture